

Design, synthesis and biological evaluations of a series of Pyrido[1,2-*a*]pyrimidinone derivatives as novel selective FGFR inhibitors



Kai Ran^{a,1}, Jun Zeng^{a,1}, Guoquan Wan^a, Xiaojie He^a, Zhazhan Feng^a, Wang Xiang^a, Wei Wei^a, Xiang Hu^a, Ningyu Wang^b, Zhihao Liu^{a,**}, Luoting Yu^{a,*}

^a State Key Laboratory of Biotherapy and Cancer Center, West China Hospital, West China Medical School, Sichuan University, And Collaborative Innovation Center for Biotherapy, 17#3rd Section, Ren Min South Road, Chengdu, 610041, China

^b School of Life Science and Engineering, Southwest JiaoTong University, Chengdu, Sichuan, 611756, China

ARTICLE INFO

Article history:

Received 3 February 2021

Received in revised form

2 April 2021

Accepted 16 April 2021

Available online 26 April 2021

Keywords:

FGFR

pyrido[1,2-*a*]pyrimidinone

Solubility

Tumor growth inhibition

ABSTRACT

Aberrant signaling of fibroblast growth factor receptors (FGFRs) has been identified as a driver of tumorigenesis and the development of many solid tumors, making FGFRs a compelling target for anti-cancer therapy. Herein, we describe the design and synthesis of pyrido[1,2-*a*]pyrimidinone derivatives as potent FGFR inhibitors. Examination of structure–activity relationships and preliminary assessment identified **23d** as a novel FGFR inhibitor that displayed excellent potency *in vitro*. Candidate **23d** suppressed the phosphorylation of FGFR signaling pathways and induced cell cycle arrest and apoptosis at low nanomolar concentration. In the kinase inhibition profile, **23d** showed excellent kinase selectivity for the FGFR family. Furthermore, **23d** showed higher aqueous solubility than Erdafitinib. Moreover, **23d** exhibited potent antitumor activity (tumor growth inhibition = 106.4%) in FGFR2-amplified SNU-16 gastric cancer xenograft model using a daily oral dose of 30 mg/kg. These results suggest that **23d** is a promising candidate for further drug development.

© 2021 Elsevier Masson SAS. All rights reserved.

1. Introduction

Fibroblast growth factor receptors (FGFRs) are composed of four highly conserved receptor subtypes (FGFR-1, 2, 3, and 4) and make up a subfamily of receptor tyrosine kinases [1]. All the FGFR subtypes consist of an extracellular ligand domain, a single transmembrane helix domain, and an intracellular domain with tyrosine kinase activity [2]. After being activated by extracellular fibroblast growth factors, FGFR undergoes dimerization and autophosphorylation, resulting in activation of downstream signaling pathways, such as PI3K-Akt, RAS-MEK-ERK, and PLC γ pathways. These FGFR cascades play important roles in cell proliferation, differentiation, and metastasis [3–6].

Abnormal FGFRs caused by gene amplifications, translocations,

and mutations in the exons of FGFR family members are associated with tumor cell invasion, metastasis, angiogenesis, tumor recurrence, and drug resistance [2,7–10]. FGFR genomic aberrations have been identified in many types of tumors [11–13]. For instance, FGFR1 amplifications occur in about 20% of squamous non-small cell lung carcinomas and 10%–15% of breast cancers. FGFR2 translocations occur in 14% of intrahepatic cholangiocarcinomas. FGFR3 mutations have been identified in 60%–80% of non-muscle-invasive bladder carcinomas, and FGFR3 translocations are also found in 3% of glioblastomas and about 20% of myelomas. In addition, FGFR4 amplifications occur in 50% of hepatocellular carcinomas. All these gain-of-function alterations result in the over-activation of downstream growth and proliferation signaling pathway and promotion of tumorigenesis. Therefore, the FGFR signaling pathway represents a promising target for cancer therapeutics.

The early FGFR inhibitors, such as Dovitinib [14], Ponatinib [15], and Lucitanib [16], usually inhibit a broad range of additional kinases. Although therapies based on inhibiting multiple kinases have been approved for the treatment of cancers, serious adverse effects such as VEGFR-2 based dose-limiting toxicities prevent their extensive clinical application [17]. To overcome these drawbacks,

* Corresponding author. Lab of Medicinal Chemistry, State Key Laboratory of Biotherapy and Cancer Center, West China Hospital, Sichuan University and Collaborative Innovation Center for Biotherapy, 17#3rd Section, Ren Min South Road, Chengdu, 610041, China.

** Corresponding author.

E-mail addresses: liuzhihao@scu.edu.cn (Z. Liu), yuluot@scu.edu.cn (L. Yu).

¹ These authors contribute equally to this work.

the second-generation FGFR kinase inhibitors with improved target selectivity were developed, of which several candidates have entered clinical trials, including NVP-BGJ398 [18] (**1**), AZD4547 [19] (**2**), LY2874455 [20] (**3**), CH5183284 [21] (**4**), Pemigatinib [22] (**5**), and Erdafitinib [23] (**6**) (Fig. 1). The recent approval of two pan-FGFR inhibitors Erdafitinib and Pemigatinib has further validated the feasibility of FGFRs inhibitors as therapeutic strategies for FGFR-related cancers [24,25].

Despite the advances made in selective FGFR inhibitors, the clinical efficacy of current FGFR inhibitors is still unsatisfactory [26–29]. Except for the lack of appropriate biomarkers for FGFR inhibitor sensitivity, the commonly reported challenge of FGFR inhibitor efficacy is the development of drug resistance. The intrinsic or acquired point mutations in the FGFR kinase domain give the current FGFR inhibitors distinct effects for different mutants. The other barrier limiting the clinical applications of FGFR inhibitors is that of adverse toxicity, including hyperphosphatemia and eye disorders, which has led to a narrow therapeutic window. These undesired side effects are closely related to the target selectivity and pharmacokinetic properties of current FGFR inhibitors [30–33]. Hence, currently medicinal chemists have focus on developing structural diversification of highly selective and highly bioactive FGFR inhibitors with potential druggability to overcome above shortcomings [34,35]. In this study, we designed and synthesized a series of pyrido[1,2-*a*]pyrimidinone derivatives as potent FGFR inhibitors with excellent potency and selectivity. The compounds displayed significant antitumor efficacy and improved aqueous solubility compared with approved drug Erdafitinib.

2. Molecular design

While Erdafitinib, the first FGFR-selective compound approved by the US Food and Drug Administration, provides encouraging clinical benefit in cancer patients harboring FGFR genetic alterations, its dose-limiting adverse events are also reported in its instruction [24]. Except for hyperphosphatemia caused by the on-target effect (unwanted inhibition of FGFR1 and FGFR3), other drug-related adverse events might be related with its unsatisfactory pharmacokinetic profile, such as long half-life ($t_{1/2}$ = 59 h) and excessive metabolic stability, which result in its accumulation *in vivo* [36]. The poor aqueous solubility of Erdafitinib (practically

insoluble at pH 7.4) is one of the main factors affecting its pharmacokinetics [37]. Therefore, measures to increase the aqueous solubility of compounds would be considered in our following design and optimization studies.

In 2014, Astex Pharmaceuticals discovered quinazolinone compound **7** as an analogue of Erdafitinib [38], but observed a 40-fold decrease in FGFR1 potency. In the co-crystal structure of FGFR1 in complex with Erdafitinib (PDB ID: 5EW8, Fig. 2A) [31], the quinoxaline core of Erdafitinib can form a single hydrogen bond with Ala564 in hinge region, while one of the methoxyl oxygen atoms in dimethoxyphenyl ring is involved in a hydrogen bond with Asp641. The methyl pyrazole group could extend towards the solvent channel and make van der Waals interactions with Lue484. In order to find out the reason for the decline in FGFR1 activity of **7** compared with Erdafitinib, we conducted a molecular docking analysis to elucidate the interaction mode of compound **7** with FGFR1 (PDB ID: 5EW8). As shown in Fig. 2B, compound **7** has a similar binding mode with Erdafitinib, and maintains the key H-bonding network observed in the complex of Erdafitinib with FGFR1. However, the nitrogen bridge in compound **7** tends to force the methyl pyrazole ring to be perpendicular to the quinazolinone core, similar to that observed in Idelalisib [39] and BMS-777607 [40]. Such perpendicular rotation of the methyl pyrazole ring would destroy its interaction with residue Lue484, leading to a decline in activity.

In view of the structural similarities between **7** and Erdafitinib, we utilized the scaffold hopping strategy [41] to design the pyrido [1,2-*a*]pyrimidinone core, which can form similar hydrogen bond with FGFR1 and might restore the interaction between adjacent aryl and residue Lue484 due to more suitable bond angle, to generate a novel type of FGFR inhibitor **8** (Fig. 2C). Furthermore, a hydrophilic group was introduced at the Ar or R₃ position of **8** in an effort to improve its solubility.

3. Chemistry

3.1. Synthesis of compounds **8a–8d**

The synthetic route to compounds **8a–8d** is shown in Scheme 1. Under Brederick reaction conditions, commercially available methyl 2-(benzyloxy)acetate **9** was converted to enamine **10**. Cyclization of **10** with 2-amino-5-bromopyridine at 90–100 °C

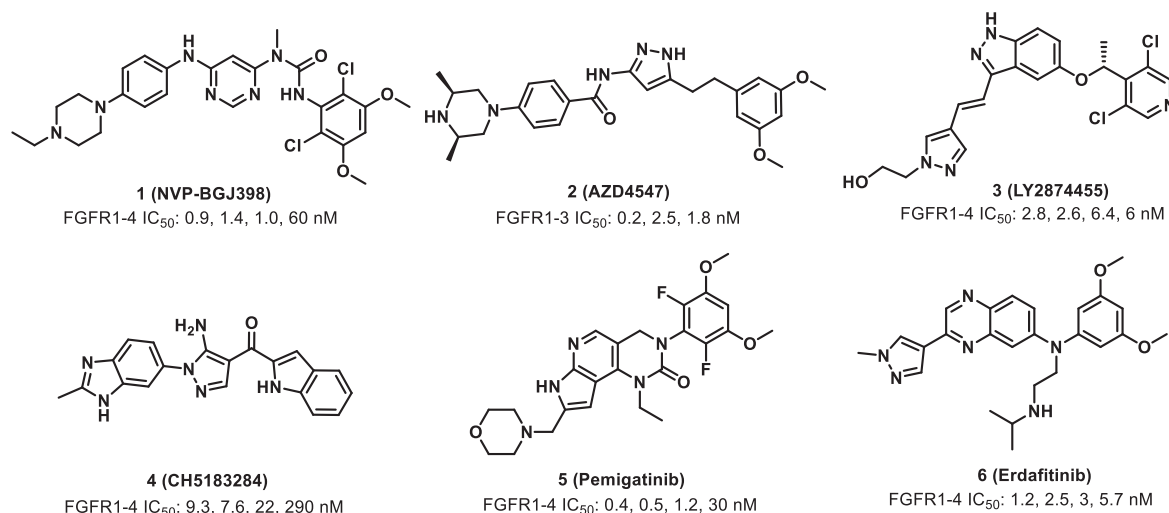


Fig. 1. Reference selective FGFR inhibitors under clinical trials or in the market.

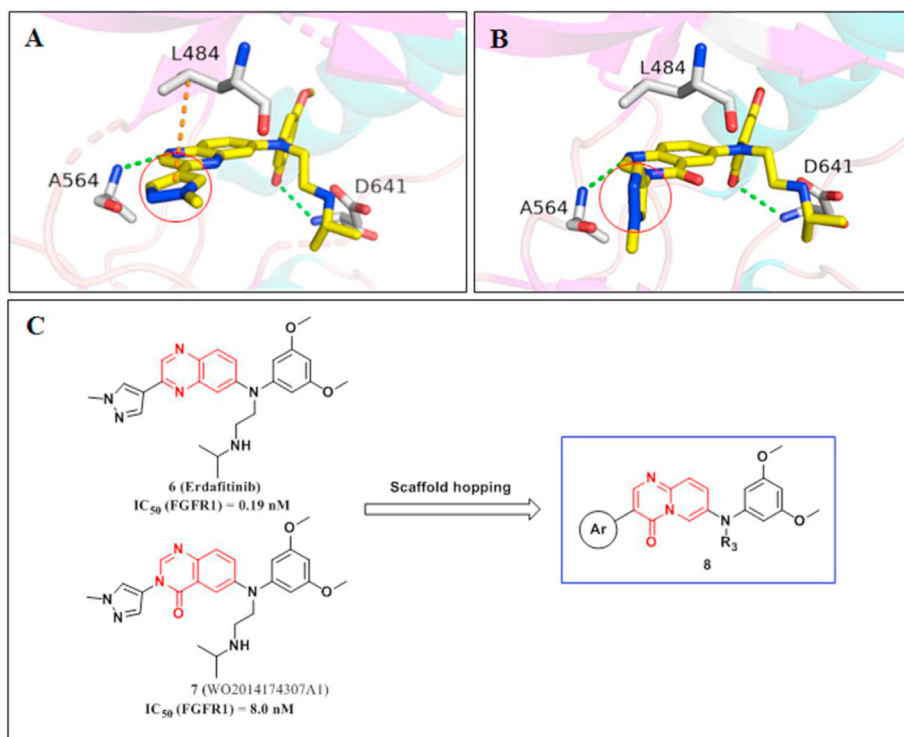
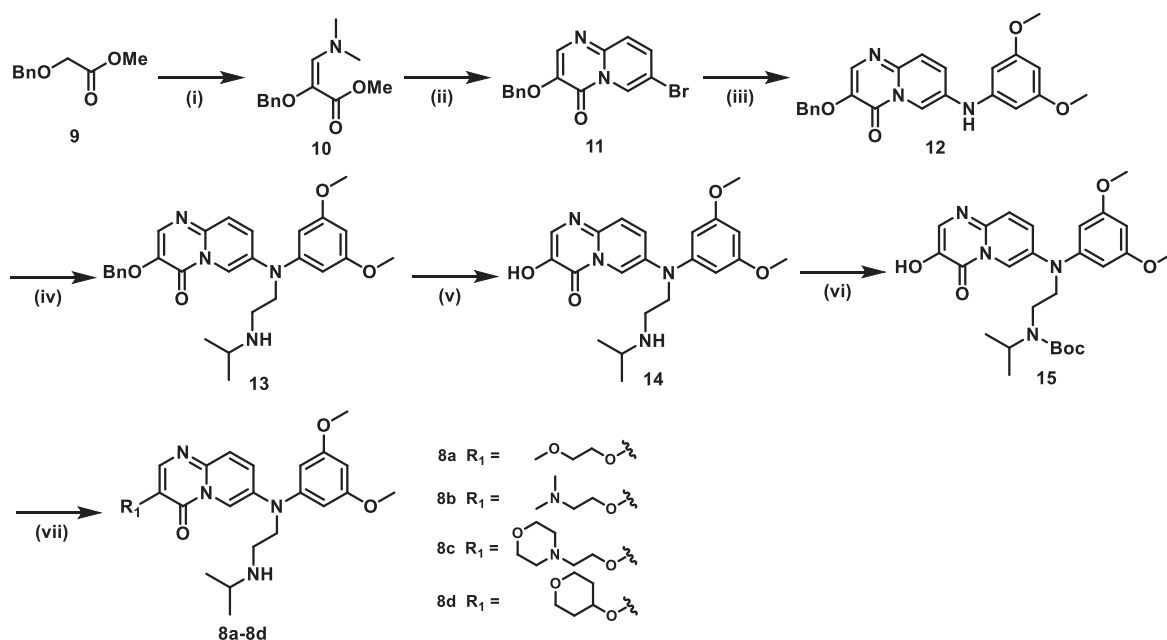


Fig. 2. (A) Cocystal structure of Erdafitinib bound with FGFR1 (PDB ID: 5EW8) [31]; (B) Docking results of **7** in the FGFR1 protein (PDB ID: 5EW8); (C) The design of pyrido[1,2-a]pyrimidinone derivatives as novel FGFR inhibitors using a scaffold hopping strategy.



Scheme 1. Reagents and conditions: (i) tert-butoxybis(dimethylamino)methane, 90 °C–100 °C; (ii) 2-amino-5-bromopyridine, AcOH, 120–130 °C; (iii) 3,5-dimethoxyaniline, Pd₂(dba)₃, BINAP, Cs₂CO₃, toluene, 100 °C; (iv) 2-isopropylaminoethylchloride hydrochloride, KOH, Bu₄NBr, THF, H₂O, 50 °C; (v) TFA, 90–100 °C; (vi) (Boc)₂O, Et₃N, THF, 0 °C–rt; (vii) (a) alkyl halide, K₂CO₃, DMF, 90–120 °C, (b) TFA, DCM, rt.

provided 3-(benzyloxy)-7-bromo-4H-pyrido[1,2-a]pyrimidin-4-one **11**. Buchwald-Hartwig cross-coupling of **11** with 3,5-dimethoxyaniline followed by nucleophilic substitution with 2-isopropylaminoethylchloride under basic conditions led to **13**. Intermediate **15** was then prepared by debenzoylation of **13** in the

presence of trifluoroacetic acid and subsequent protection with a Boc group. Finally, the target compounds **8a–8d** were obtained through substitution of **15** with different alkyl halides and subsequent Boc deprotection.

3.2. Synthesis of compounds **23a–23m**

Synthesis of compounds **23a–23m** is outlined in Scheme 2. Treatment of 5-bromopyridin-2-amine **17** with 2,2-dimethyl-1,3-dioxane-4,6-dione in the presence of triethyl orthoformate, followed by cyclization in diphenyl oxide at 220 °C led to 7-bromo-4*H*-pyrido[1,2-*a*]pyrimidin-4-one **19**. Iodination of **19** at the α -position of the amide using *N*-iodosuccinimide gave dihalogenated intermediate **20**. Subsequent Suzuki reaction with different boronic esters and Buchward coupling with 3,5-dimethoxyaniline afforded **22a–22m**. Compounds **23a–23m** were prepared by nucleophilic substitution of **22a–22m** with 2-isopropylaminoethylchloride under basic conditions, after which **23b** and **23g** underwent additional deprotection in the presence of hydrochloric acid.

3.3. Synthesis of compounds **27a–27f** and **29a–29f**

Scheme 3 presents the synthesis of compounds **27a–27f** and **29a–29f**. Starting from intermediate **23l**, benzyloxycarbonyl (CBZ) protection of the free amine and subsequent selective tetrahydropyranyl deprotection produced the pyrazole **25**. Treatment with different alkyl halides or alkylene oxides afforded **26a–26f**, which were converted to the target compounds **27a–27f** via removal of all protective groups in the presence of hydrobromic acid. Meanwhile, the selective Boc deprotection of **26e** and **26f** in the presence of trifluoroacetic acid provided **28a** and **28b**, respectively. Reductive amination of **28a** with different aldehydes followed by CBZ deprotection gave compounds **29a** and **29b**. Acylation or methanesulfonylation of **28a** and **28b** followed by CBZ deprotection yielded **29c–29f**.

3.4. Synthesis of compounds **30a**, **30b**, **32**, and **34a–34c**

As shown in Scheme 4, nucleophilic substitution of **22d** with different alkyl halides in the presence of NaH provided **30a** and **30b**. Using the same method, treatment of **22d** with (2-bromoethoxy)(*tert*-butyl)dimethylsilane afforded intermediate **31**, which was then converted to compound **32** via TBDMS (*tert*-butyldimethylsilyl) deprotection in the presence of tetrabutylammonium fluoride. Next, methanesulfonylation of alcohol **32** followed by displacement of the resulting methanesulfonyloxy

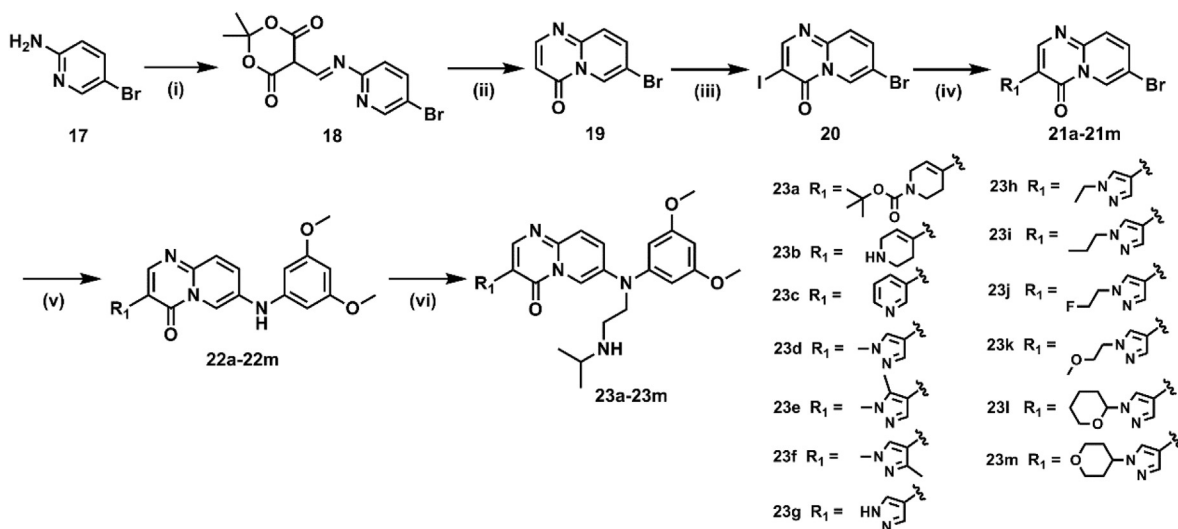
leaving group with various amines furnished target compounds **34a–34c**.

4. Results and discussion

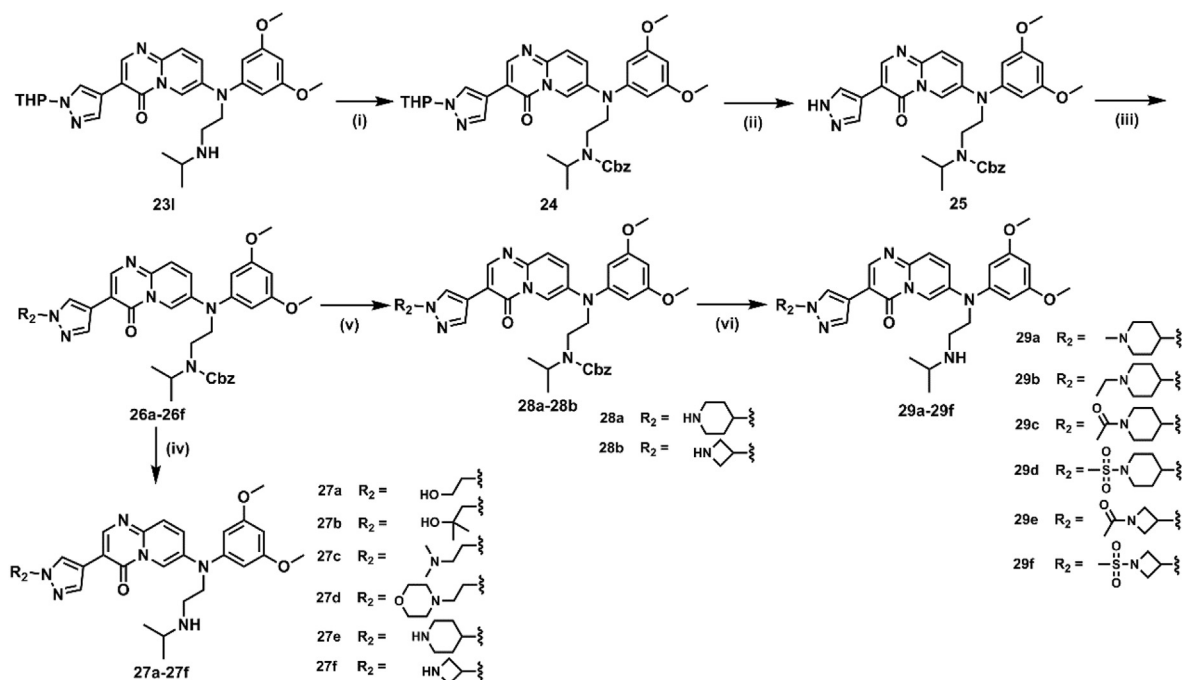
4.1. Structure–activity relationships

All the synthetic compounds were assayed for their biochemical activity against FGFR1. Potent compounds were further tested for their antiproliferative effects in FGFR2-amplified SNU-16 cells. Erdafitinib was used as the positive control. We first focused on optimizing the R_1 group adjacent to the pyrido[1,2-*a*]pyrimidinone core by introducing different substituents (see Table 1). Compounds **8a–8d** were obtained by introduction of flexible alkoxy groups at the R_1 position, and all of them showed a complete loss in FGFR1 inhibitory activity. When R_1 was substituted by a partially saturated ring, the activity of the *N*-Boc protected tetrahydropyridine ring **23a** and corresponding deprotected amine **23b** increased. Inspired by this result, the aromatic heterocycle methyl pyrazole (**23d**), dimethyl-substituted pyrazoles (**23e** and **23f**), and pyrazole (**23g**) were introduced at the same position. Among these compounds, **23d** and **23g** exhibited the most potent enzymatic and cellular activity with IC_{50} values below 10 nM. Notably, **23d** showed the highest potency against FGFR1 (IC_{50} = 0.57 nM) and SNU-16 (IC_{50} = 3.3 nM). Accordingly, based on the pyrazol-4-yl group, a series of *N*-substituents on the pyrazole ring were prepared in the search for a more effective compound. All the extended *N*-substituents (**23h–23k**) displayed good FGFR1 inhibition with IC_{50} values ranging from 1.0 to 8.0 nM. Of these compounds, 2-fluoroethyl **23j** had the highest antiproliferative effect (IC_{50} = 1.9 nM), probably because of its good cell permeability. Likewise, **23l** and **23m** featuring bulky tetrahydropyranyl groups maintained good potency in both enzymatic and cellular activity.

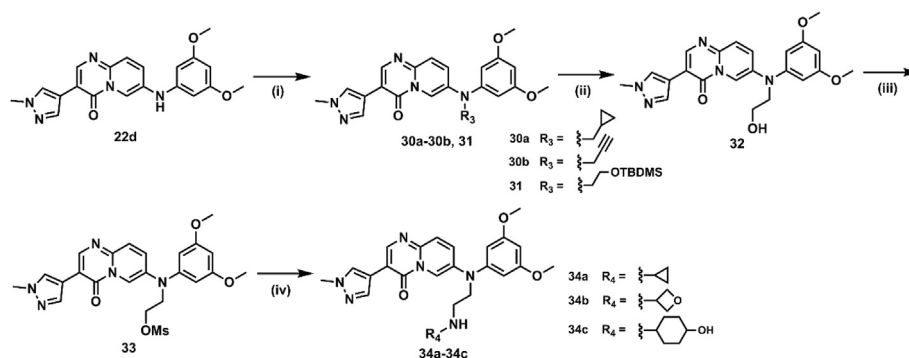
Motivated by good tolerance of *N*-substituents on the pyrazol-4-yl group described above, incorporation of a polar group or a basic center at this position was performed in the following optimization to improve the solubility (see Table 2). All the obtained compounds maintained good potency against FGFR1 and SNU-16 cells. Consistent with our expectation, hydroxyethyl **27a** showed about 5-fold improvement in aqueous solubility (147 μ g/mL) compared with Erdafitinib. When two methyl groups were further introduced



Scheme 2. Reagents and conditions: (i) Triethyl orthoformate, 2,2-dimethyl-1,3-dioxane-4,6-dione, EtOH, reflux; (ii) Diphenyl oxide, 220 °C; (iii) NIS, DMF, 80 °C; (iv) Boronic acids or boronate esters, PdCl₂DPPF, K₂CO₃, dioxane, H₂O, 100 °C; (v) 3,5-Dimethoxyaniline, Pd₂(dba)₃, 2,2'-bis(diphenylphosphino)-1,1'-dinaphthalene, Cs₂CO₃, toluene, 100 °C; (vi) (a) 2-Isopropylaminoethylchloride hydrochloride, KOH, Bu₄NBr, THF, H₂O, 50 °C; (b) HCl, dioxane, rt.



Scheme 3. Reagents and conditions: (i) CbzCl, DIEA, DCM, rt; (ii) 5 N HCl, MeOH, rt; (iii) alkyl halide, Cs₂CO₃, DMF, 100 °C; (iv) HBr, AcOH, rt; (v) TFA, DCM, rt; (vi) (a) aldehyde, AcOH, Na(OAc)₃BH, 1,2-dichloroethane, rt-60 °C; (b) HBr, AcOH, rt or (c) acyl chloride/sulfonyl chloride, Et₃N, DCM, rt; (d) HBr, AcOH, rt.



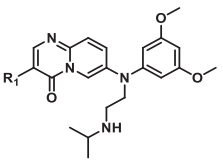
Scheme 4. Reagents and conditions: (i) alkyl halide, NaH, DMF, 5 °C-rt; (ii) TBAF, THF, rt; (iii) MsCl, Et₃N, CH₂Cl₂, 0 °C; (iv) amine, CH₃CN, 100 °C.

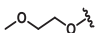

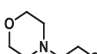
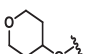
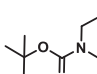
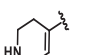
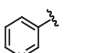
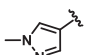
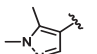
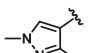
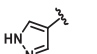
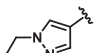
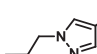
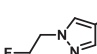
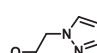
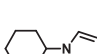
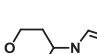
on the hydroxyethyl tail (**27b**), a 3-fold lower solubility (49.4 µg/mL) was observed. The introduction of a basic center (**27c** and **27d**) did not increase the solubility. Then we attempted to connect the pyrazole ring with an unsubstituted piperidine ring. The resulting compound **27e** showed an obvious improvement in solubility (227 µg/mL) but showed a slight decrease in cellular activity, which was probably caused by decreased cell permeability. Further modification of the piperidine ring with methyl (**29a**) and ethyl (**29b**) groups slightly increased the antiproliferative potency, but also resulted in significantly decreased solubility. To our surprise, acetylpyridinyl **29c** and (methylsulfonyl)piperidinyl **29d** exhibited both high potency and significantly improved solubility. Notably, **29d** achieved the highest cellular activity (IC₅₀ = 0.67 nM) and aqueous solubility (227 µg/mL). In addition, we used azetidine instead of piperidine to prepare similar compounds **27f**, **29e**, and **29f**; however, none showed better potency or solubility than compound **29d**. Despite the encouraging profiles for activity and solubility, the molecular weight of **29d** (MW = 610) exceeded 500, which caused some concern for its pharmacokinetic properties. In a

retrospective determination, the previous highly active compound **23d** showed better solubility (327 µg/mL), and its molecular weight was less than 500.

We analyzed the co-crystal structure of Erdaftinib/FGFR1 complex and found that the 2-isopropylaminoethyl chain in Erdaftinib could extend away from the kinase domain into a solvent exposed region [34]. Hence, introduction of some polar or hydrophilic groups at this position of **8** would have the potential to improve the compound's solubility while maintaining its activity. Given that the *N*-methyl substitution on pyrazole ring provided the most potent inhibition against FGFR1 and the highest solubility, the scaffold 7-[(3,5-dimethoxyphenyl)amino]-3-(1-methyl-1*H*-pyrazol-4-yl)-4*H*-pyrido[1,2-*a*]pyrimidin-4-one was established for the following investigation of R₃ variations. However, all the obtained derivatives (**30a–30b**, **32** and **34a–34c**) showed slightly or apparently lower potency against FGFR1 or cellular activity compared with **23d**. Overall, with good enzymatic activity, cellular activity, and aqueous solubility, compound **23d** was chosen for further evaluation.

Table 1
Structure–activity results for chemical modifications at R₁.



Compound	R ₁	IC ₅₀ (nM)	
		FGFR1 ^a	SNU-16 cell ^b
8a		>100	N.T. ^c
8b		>100	N.T.
8c		>100	N.T.
8d		>100	N.T.
23a		3.7	17.7
23b		22	59.9
23c		37	53.2
23d		0.57	3.3
23e		>100	N.T.
23f		50	N.T.
23g		2.1	7.3
23h		8.0	32.4
23i		1.0	3.5
23j		1.2	1.9
23k		2.0	6.9
23l		1.2	4.7
23m		1.5	1.8
Erdaftinib		0.19	1.1

^a Biochemical assay was performed with ATP at K_m concentration, test results provided by Sundia MediTech Company, Ltd.

^b Tumour cells were treated with compounds for 72 h.

^c N.T.: Not tested.

4.2. Kinase selectivity profile of **23d**

For a broad assessment of the kinase selectivity, **23d** was evaluated kinase inhibition profile against a diverse panel of 360 recombinant human kinases from Eurofins Discovery using an *in vitro* ATP-site competition binding assay at a concentration of 1 μM. As summarized in Fig. 3 (a list of the tested kinases can be found in Table S1) [16], kinases were inhibited at a cutoff of 35% of the dimethyl sulfoxide control. Of these, only 9 hits (FGFR1, FGFR2, FGFR3, FGFR4, RET, FLT1, FLT4, Lyn, and FMS) including FGFR1–4 had >90% inhibition. Further FGFR1–4 enzymatic assay displayed potent inhibition with IC₅₀s of 0.57, 2.0, 0.80 and 1.4 nM, respectively. All these data indicated that **23d** was a potent and selective pan-FGFR inhibitor.

4.3. Molecular docking of **23d**

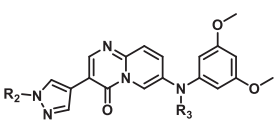
To elucidate the mode of interaction of **23d** with FGFR, we conducted molecular docking analysis using a reported crystal structure of FGFR1 (PDB ID: 5EW8). As illustrated in Fig. 4A, **23d** showed a binding mode similar to that of Erdaftinib (**6**) and maintains the key H-bonding network observed in the complex of FGFR1 with **6**, as shown in Fig. 2A. In terms of the difference between the two complexes, the pyrazole ring of **23d** could undergo some rotation with respect to the pyrido[1,2-*a*]pyrimidinone core (Fig. 4C), while the pyrazole ring of **6** was coplanar with the quinoxaline ring [31] (Fig. 4B). Fortunately, the slight rotation of the pyrazole ring in **23d** did not affect its interaction with amino acid residue Lue484, which resulted in improved enzymatic potency when compared with the lead **7** (Fig. 2B). Furthermore, this rotation disrupted the planarity of compound **23d**, which may have been a factor its higher aqueous solubility when compared with **6**.

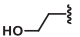
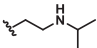
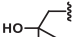
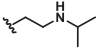
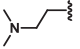
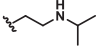
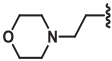
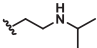
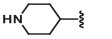
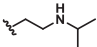
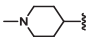
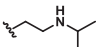
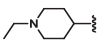
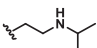
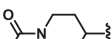
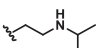
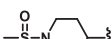
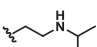
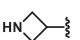
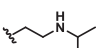
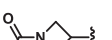
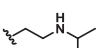
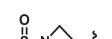
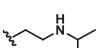
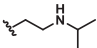

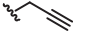
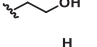
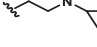
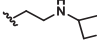
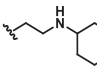
4.4. Inhibition on FGFR signaling by compound **23d**

To investigate the cellular effects of compound **23d** in targeting FGFR signaling pathway, the effects of **23d** on the phosphorylation of FGFR and its major downstream signaling molecules were analyzed by Western blot in SNU-16 cells (FGFR2-amplification). As shown in Fig. 5, the phosphorylation of FGFR2 was obviously inhibited by **23d** in a dose-dependent manner. Besides, **23d** significantly inhibited the phosphorylation of FRS2. The phosphorylation of AKT and ERK1/2 was also decreased at 5 nM concentration, indicating that PI3K-ATK and MAPK signaling were also significantly repressed.

4.5. Inhibition of SNU-16 cell proliferation by compound **23d**

Since FGFRs play a vital role in cell proliferation and survival, we examined the proliferation inhibitory effect of **23d** against FGFR2-amplified SNU-16 gastric cells using the MTT assay and a cell counting assay in detail. In the MTT assay, SNU-16 cells were exposed to graded concentrations of **23d** for 24, 48, 72, or 96 h, and caused marked decreases in viability (Fig. 6A). This showed that **23d** inhibited the proliferation of SNU-16 cells in a time-dependent and concentration-dependent manner. The following cell counting assay provided a readily visible example of cell proliferation inhibition (Fig. 6B and C). Remarkably, **23d** almost completely inhibited the growth of SNU-16 cells at 10 nM concentration, indicating its superior anti-proliferative effect *in vitro*.

Table 2Structure, activity and solubility relationships for chemical modifications at R₂ and R₃.


Compound	R ₂	R ₃	IC ₅₀ (nM)		Solubility ^c (μg/mL)
			FGFR1 ^a	SNU-16 cell ^b	
Erdafitinib			0.19	1.1	29.4
27a			2.7	9.1	147
27b			1.4	4.1	49.4
27c			1.2	5.5	<10.0
27d			1.2	4.8	<10.0
27e			0.65	15.7	227
29a			1.3	5.9	<10.0
29b			2.4	10.5	<10.0
29c			0.82	1.8	197
29d			1.0	0.67	227
27f			1.2	87.5	<10.0
29e			1.6	4.4	59.1
29f			1.6	4.0	<10.0
23d	Me		0.57	3.3	327
30a	Me		>100	N.T. ^d	N.T.
30b	Me		18	44.0	N.T.
32	Me		1.9	23.0	N.T.
34a	Me		14	28.7	N.T.
34b	Me		85	99.7	N.T.
34c	Me		2.5	12.6	N.T.

^a Biochemical assay was performed with ATP at K_m concentration; test results provided by Sundia MediTech Company, Ltd.^b Tumour cells were treated with compounds for 72 h.^c Solubility at pH 7.4.^d N.T.: Not tested.

4.6. Compound **23d** induces cell cycle G0/G1 phase arrest and apoptosis

As the inhibition of FGFR activity has the influence on cell cycle and apoptosis, we conducted flow cytometry assay (FCM) analysis

of **23d**-treated SNU-16 cells. The experimental results showed that **23d** induced both cell arrest in the G0/G1 phase (Fig. 7A and B) and cell apoptosis (Fig. 7C and D) when the concentration exceeded 5 nM. The expression of cell cycle-related proteins including CDK2, CDK4, CDK6, Cyclin D, and Cyclin E were inhibited at a similar

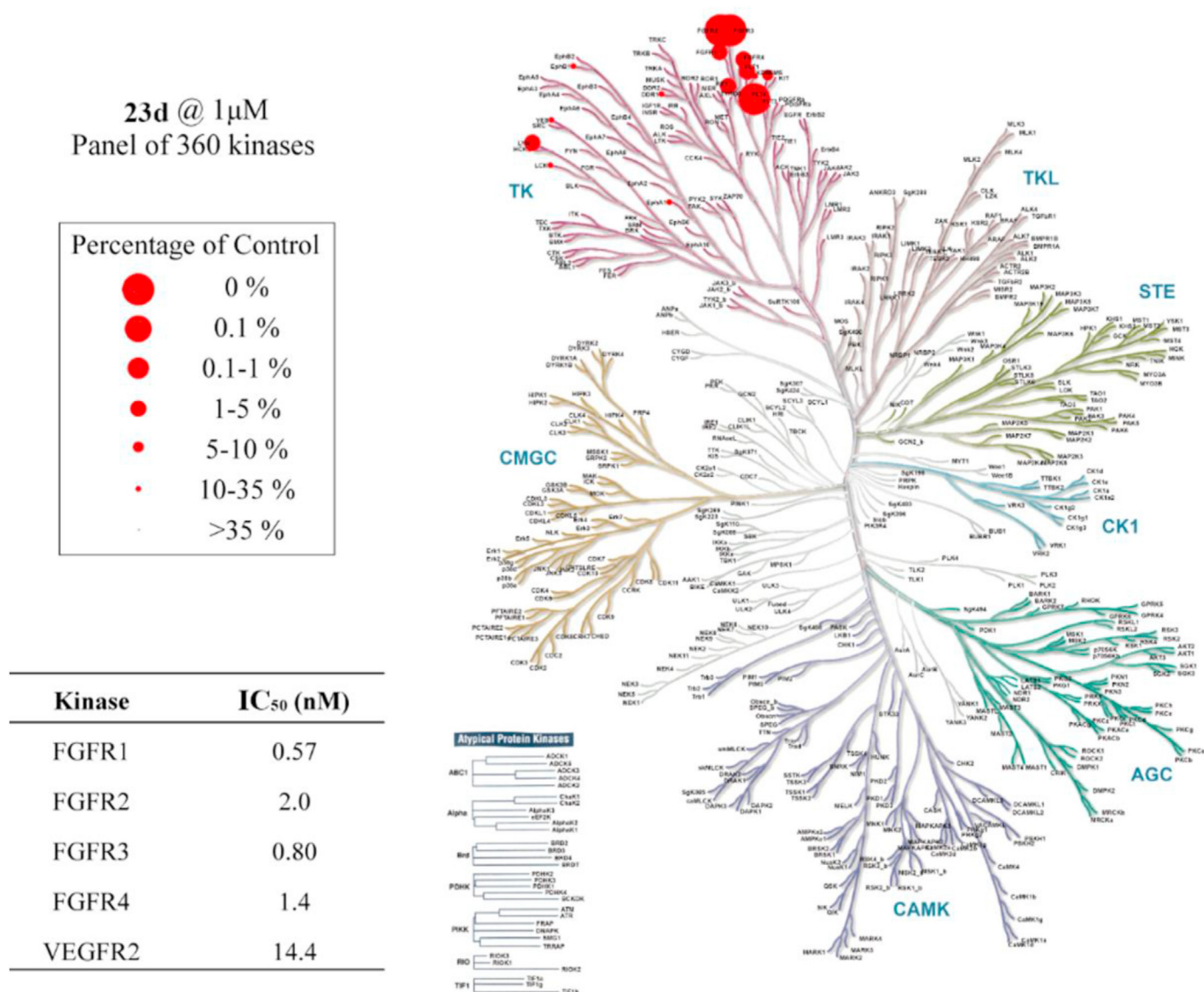


Fig. 3. Kinome-wide selectivity profiling of compound **23d** with the Kinase Profile assay by Eurofins Discovery. Measurements were performed at a concentration of 1 μ M of the inhibitor in duplicate. The % control means remaining active kinase percentage. The affinity was defined with respect to a dimethyl sulfoxide (DMSO) control. The TREEspot image was mapped with the KinMap software tool provided by Cell Signaling Technology, Inc. (www.cellsignal.com). Biochemical IC₅₀s of **23d** were determined against FGFR1-4. The results were provided by Sundia MediTech Company, Ltd., n = 1.

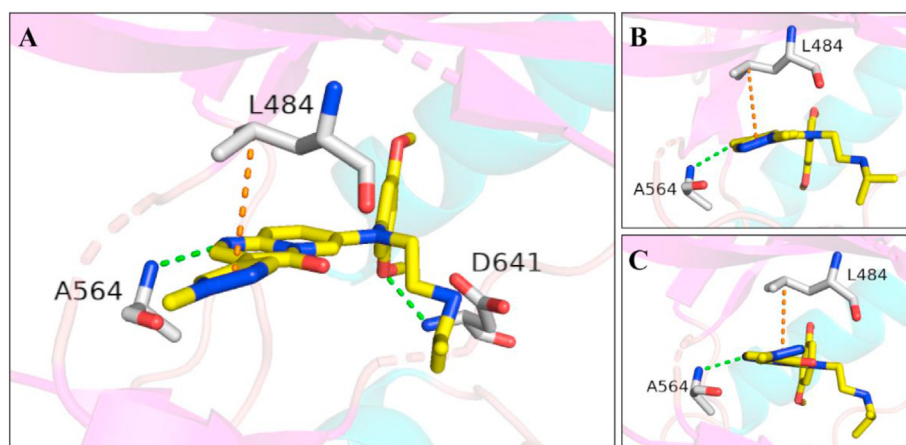


Fig. 4. (A) Docking results of **23d** in the FGFR1 protein (PDB ID: 5EW8); (B) Cocystal structure of **6** bound to FGFR1 (PDB ID: 5EW8) [31]; (C) Rotation of (A).

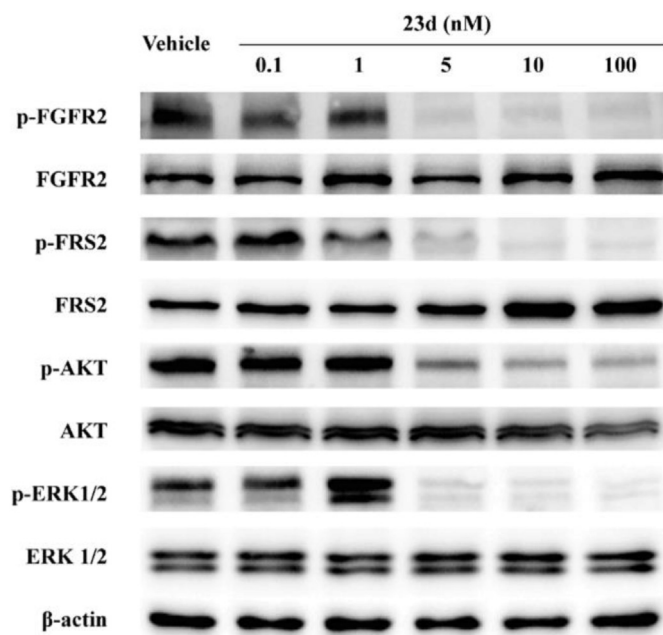


Fig. 5. Compound **23d** effectively inhibits the phosphorylation of FGFR2 and the downstream effectors FRS2, AKT and ERK1/2 in SNU-16 cells. Cells treated with **23d** for 24 h at the indicated concentrations were lysed and subjected to Western blot analysis.

concentration (Fig. 7E), and upregulation of apoptosis-related proteins, including cleaved caspase-9 and cleaved PARP, was also observed (Fig. 7F).

4.7. Pharmacokinetic study of compound **23d**

Before *in vivo* efficacy evaluation, the pharmacokinetic profile of the pan-FGFR inhibitor **23d** was tested in Sprague-Dawley rats (iv, 3 mg/kg; oral, 30 mg/kg). Blood samples were collected at 0.083, 0.16, 0.25, 0.5, 1, 2, 4, 6, 10, and 24 h after dosing. The blood drug level was then determined with liquid chromatography–tandem mass spectrometry. The pharmacokinetic parameters are listed in Table 3. In rats, **23d** showed slow absorption ($T_{max} = 4.33$ h), with a peak concentration of 130.34 ng/mL, an AUC value of 948.37 ng h/mL, and a terminal half-life of 2.65 h following a single oral dose of 30 mg/kg. The oral bioavailability of **23d** in rat was 14.94%.

4.8. *In vivo* antitumor efficacy in human xenografts of **23d**

Given that compound **23d** showed good kinase selectivity, excellent activity, and acceptable pharmacokinetic properties, the efficacy of **23d** *in vivo* was tested in the SNU-16 xenograft model. **23d** was orally administered at doses of 15 or 30 mg/kg once daily for 4 weeks. The results showed that **23d** could suppress tumor growth in a dose-dependent manner, with tumor growth inhibition of 67.3% and 106.4% at the doses of 15 and 30 mg/kg, respectively

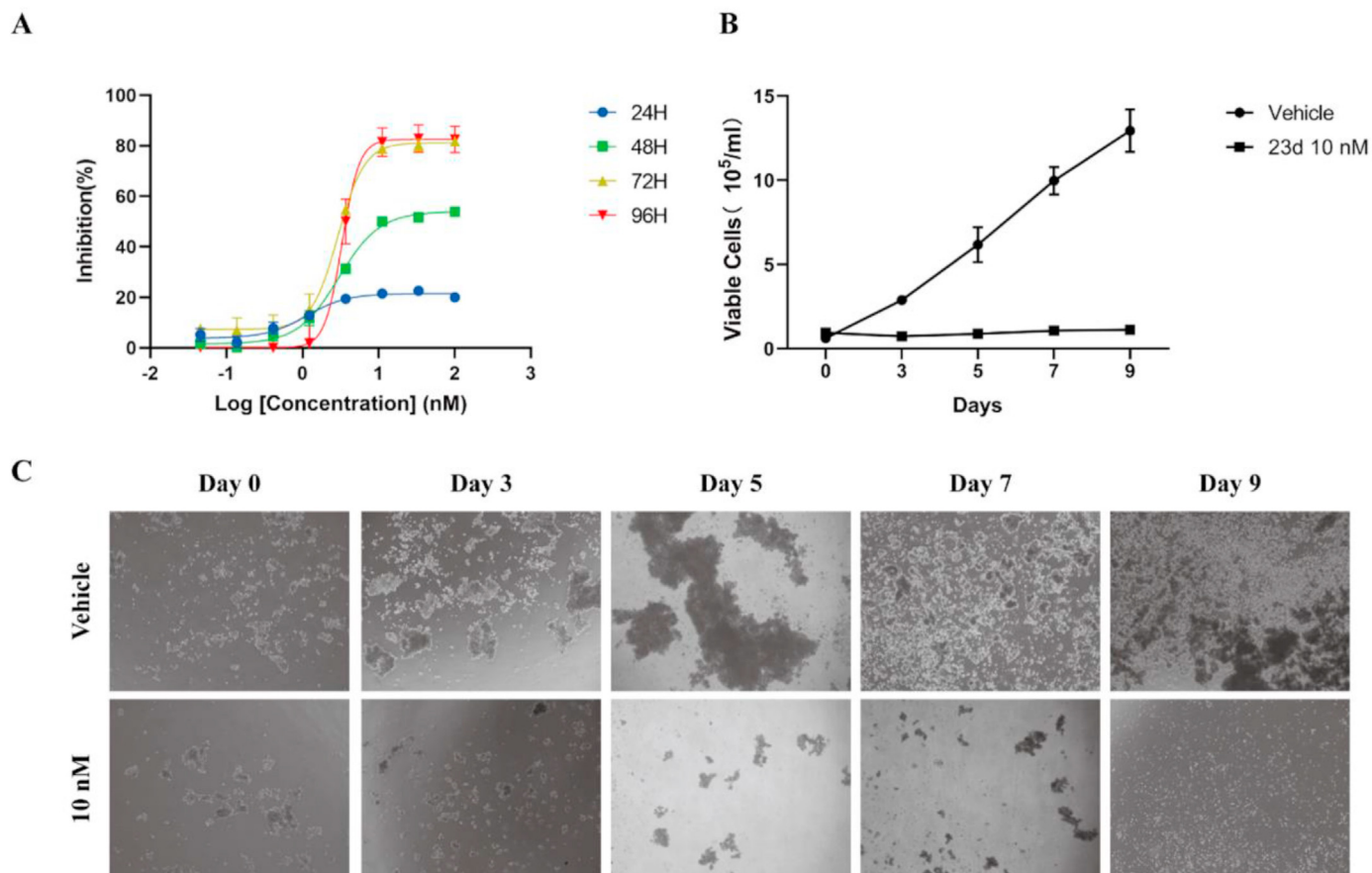


Fig. 6. Antiproliferative effect of **23d** on SNU-16 cells. (A) SNU-16 cell lines were treated with different concentrations of **23d** for 24 h, 48 h, 72 h, and 96 h, respectively; (B) The statistics of cell counting; (C) Photographs of cell counting at different time after 10 nM treatment of **23d**.

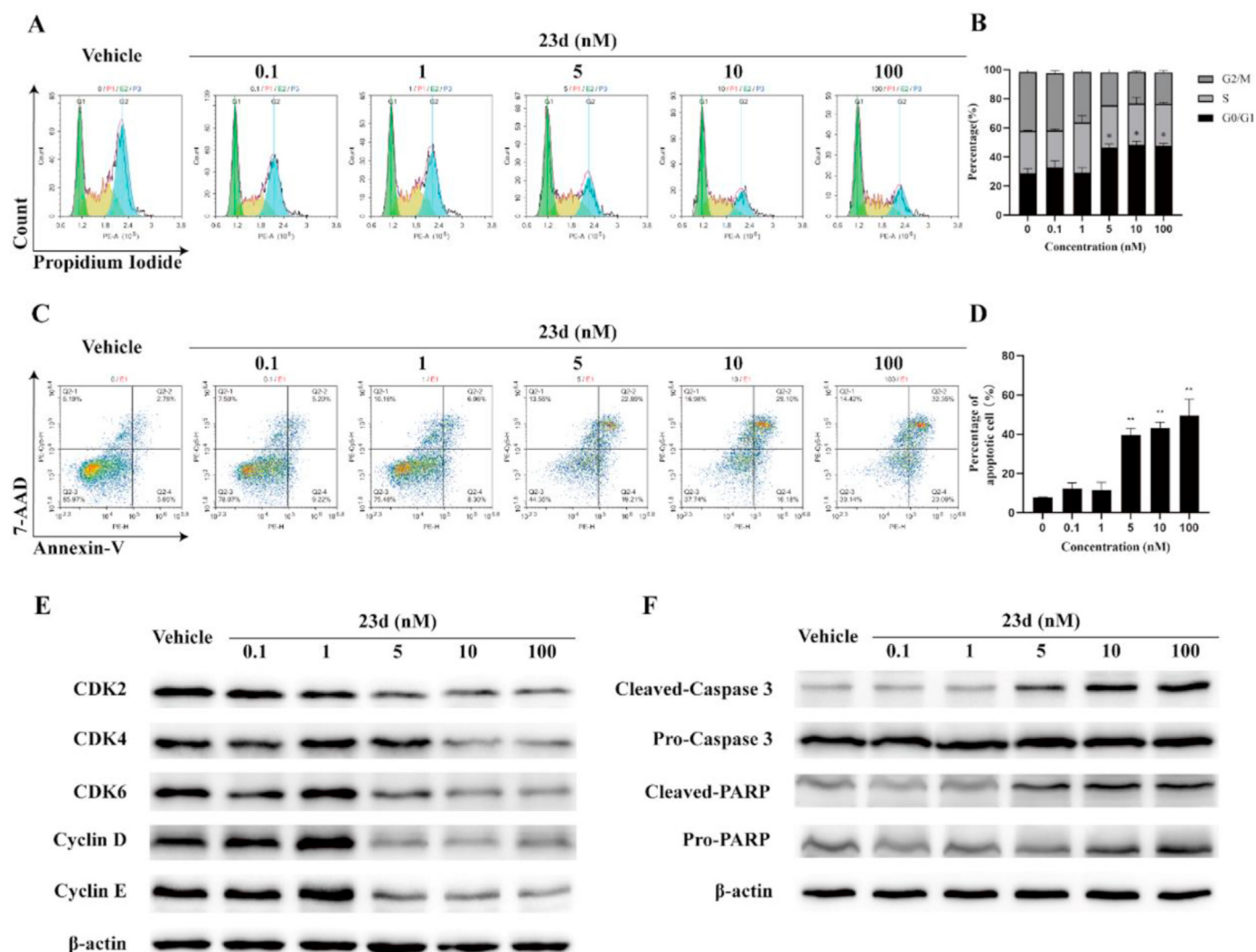


Fig. 7. (A) FCM analysis for cell cycle effects of **23d** on SNU-16 cells. Cell were treated with increasing concentration of **23d** for 48 h, harvested, fixed and stained with propidium iodide; (B) Data analysis for cell cycle FCM analysis (*, $p < 0.05$); (C) FCM analysis for apoptosis effects of **23d**. SNU-16 cells were treated with **23d** for 72 h with increasing concentration, followed by staining with 7-AAD/Annexin V; (D) Data analysis for cell apoptosis FCM analysis (**, $p < 0.01$, ***, $p < 0.001$); (E) Immunoblotting analysis of cell cycle related protein expression after 48 h of treatment of **23d**; (F) Immunoblotting analysis of apoptosis related protein expression after 72 h of treatment of **23d**. Each experiment was repeated three times.

Table 3
Pharmacokinetic profiles of **23d** in rats.

Doses (mg/kg)	C_{max} (ng/mL)	T_{max} (h)	AUC_{0-t} (ng·h/mL)	MRT (h)	$T_{1/2}$ (h)	F%
3 mg/kg iv	466.20 ± 96.14	0.08 ± 0.00	634.76 ± 118.47	1.38 ± 0.15	1.39 ± 0.25	
30 mg/kg po	130.34 ± 76.51	4.33 ± 4.93	948.37 ± 370.10	5.29 ± 2.41	2.65 ± 0.89	14.94%

(Fig. 8A). The final average tumor weight in the treated group was much lower than that of the vehicle-treated group (Fig. 8C). In addition, no significant change of body weight (Fig. 8B) or blood biochemical parameters (Fig. 8D and E) were observed after **23d** treatment. Therefore, **23d** can be considered an effective and safe FGFR inhibitor candidate that is suitable for further drug development.

5. Conclusion

This article describes the design, synthesis, and biological evaluation of a series of pyrido[1,2-*a*]pyrimidinone derivatives as

novel selective FGFR inhibitors. Systematic exploration and optimization of several substitutions on the pyrido[1,2-*a*]pyrimidinone scaffold led to the identification of optimal compound **23d**. The incorporation of pyrido[1,2-*a*]pyrimidinone in **23d** afforded the pyrazole ring slight rotation while retaining its interaction with amino acid residue Lue484 of FGFR1. This led to increased potency against FGFR1 when compared with the lead **7**. The small rotation of pyrazole ring may also be helpful to improve the aqueous solubility of **23d** compared with Erdafitinib by disrupting its molecular planarity. Full kinase spectrum screening indicated that **23d** possessed relatively high selectivity against the FGFR family. Western blot assay also confirmed that the antitumor activities

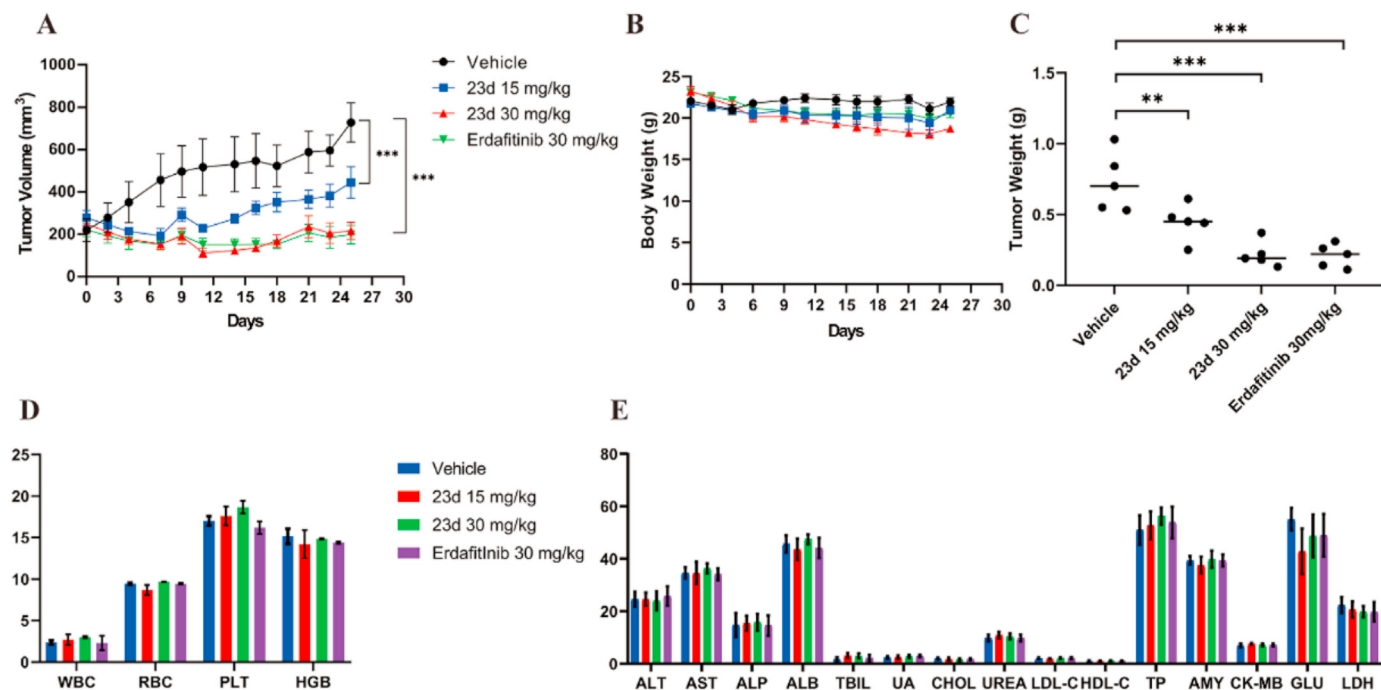


Fig. 8. In-vivo efficacy of **23d** in SNU-16 xenograft model. NOD/SCID mice bearing SNU-16 ($n = 5$) were treated with vehicle control, Erdafitinib (30 mg/kg) and **23d** (15 mg/kg and 30 mg/kg) once per day for 4 weeks. (A) Tumor volumes were measured three times per week (***, $p < 0.001$, two-way ANOVA); (B) Tumor weight after 4 weeks of treatment (**, $p < 0.01$, ***, $p < 0.001$, t -test); (C) Body weight change in SNU-16 xenograft during treatment; (D) CBC analysis after treatment (Unit for WBC, RBC, PLT, HGB is $10^9/L$, $10^{12}/L$, $10^{11}/L$, 10 g/L , respectively); (E) Blood biochemical analysis after treatment.

were indeed on-target. Furthermore, compound **23d** stimulated tumor cell cycle arrest in the G0/G1 phase and induced apoptosis at low nanomolar concentration. After oral administration of compound **23d** at a daily dose of 30 mg/kg, almost complete tumor stasis was observed in nude mice bearing SNU-16 human gastric cancer xenograft after 4 weeks of initial administration. These results highlight the status of **23d** as a promising FGFR inhibitor for further drug development.

6. Experimental section

6.1. Chemistry

Unless otherwise noted, all materials were obtained from commercial suppliers and used without further purification. The ¹H and ¹³C NMR spectra were recorded on a Bruker Avance 400 spectrometer at 25 °C using DMSO-*d*₆ or CDCl₃ as the solvent. Chemical shifts (δ ppm) are reported in ppm relative to Me₄Si (internal standard), coupling constants (J Hz) are reported in hertz, and peak multiplicity are reported as s (singlet), d (doublet), t (triplet), q (quartet), m (multiplet), or brs (broad singlet). High resolution mass analysis is performed on a Waters Q-TOF Premier mass spectrometer with electron spray ionization (ESI). Thin layer chromatography (TLC) was performed on 0.20 mm silica gel F-254 plates (Qingdao Haiyang Chemical, China). Visualization of TLC was accomplished with UV light and/or aqueous potassium permanganate or I₂ in silica gel. Column chromatography was performed using silica gel 60 of 300–400 mesh (Qingdao Haiyang Chemical, China).

6.1.1. *N*¹-(3,5-dimethoxyphenyl)-*N*²-isopropyl-*N*¹-(3-(1-methyl-1H-pyrazol-4-yl)quinoxalin-6-yl)ethane-1,2-diamine (**6**)

6 was synthesized using the procedure described in the patent application WO2011/135376A1 [42]. ¹H NMR (400 MHz, DMSO-*d*₆):

δ 8.96 (s, 1H), 8.55 (s, 1H), 8.21 (s, 1H), 7.77 (d, $J = 9.2$ Hz, 1H), 7.29 (dd, $J = 9.2$, 2.7 Hz, 1H), 7.16 (d, $J = 2.6$ Hz, 1H), 6.48 (d, $J = 2.2$ Hz, 2H), 6.42 (t, $J = 2.2$ Hz, 1H), 3.94 (s, 3H), 3.89 (t, $J = 7.0$ Hz, 2H), 3.75 (s, 6H), 2.81 (t, $J = 7.0$ Hz, 2H), 2.75–2.67 (m, 1H), 0.96 (d, $J = 6.2$ Hz, 6H). ¹³C NMR (101 MHz, DMSO-*d*₆): δ 161.90, 149.57, 148.48, 147.53, 143.98, 140.09, 138.27, 135.96, 131.18, 129.49, 121.80, 120.87, 109.58, 104.35, 97.52, 55.77, 52.86, 48.53, 44.34, 39.32, 23.38. HRMS: calculated for C₂₅H₃₀N₆O₂ [(M + H)⁺], 447.2504; found 447.2507.

6.1.2. 6-((3,5-dimethoxyphenyl)(2-(isopropylamino)ethyl)amino)-3-(1-methyl-1H-pyrazol-4-yl)quinazolin-4(3H)-one (**7**)

7 was synthesized using the procedure described in the patent application WO2014/174307A1 [38]. ¹H NMR (400 MHz, DMSO-*d*₆): δ 8.27 (s, 1H), 8.21 (s, 1H), 7.82 (s, 1H), 7.61 (d, $J = 2.8$ Hz, 1H), 7.59 (d, $J = 9.0$ Hz, 1H), 7.44 (dd, $J = 9.0$, 2.8 Hz, 1H), 6.33 (d, $J = 2.0$ Hz, 2H), 6.29 (t, $J = 2.0$ Hz, 1H), 3.91 (s, 3H), 3.83 (t, $J = 7.0$ Hz, 2H), 3.71 (s, 6H), 2.76 (t, $J = 7.0$ Hz, 2H), 2.73–2.67 (m, 1H), 0.95 (d, $J = 6.2$ Hz, 6H). ¹³C NMR (101 MHz, DMSO-*d*₆): δ 161.82, 159.43, 148.91, 147.36, 144.37, 141.02, 134.55, 128.77, 127.34, 126.36, 122.82, 120.22, 112.80, 102.23, 95.99, 55.68, 52.59, 48.51, 44.17, 39.99, 23.23. HRMS: calculated for C₂₅H₃₀N₆O₃ [(M + H)⁺], 463.2453; found 463.2456.

6.1.3. 7-((3,5-dimethoxyphenyl)(2-(isopropylamino)ethyl)amino)-3-(2-methoxyethoxy)-4H-pyrido[1,2-*a*]pyrimidin-4-one (**8a**)

Step 1: 3-(benzyloxy)-7-bromo-4H-pyrido[1,2-*a*]pyrimidin-4-one (**11**). A mixture of methyl 2-(benzyloxy)acetate (**9**, 7.0 g, 39 mmol) and Bredereck's reagent (8.2 g, 47 mmol) was stirred at 90–100 °C for 12 h. TLC detected that the reaction was completed. The mixture was concentrated in vacuo. Then the resulting solid was dissolved in AcOH (90 mL), 5-bromopyridin-2-amine (6.8 g, 39 mmol) was added. The reaction mixture was stirred at 120–130 °C for 16 h. Upon completion of the reaction, AcOH was removed under vacuum. The residue was dissolved in

ethyl acetate (40 mL). The undissolved solid was collected by filtration, washed with a small amount of ethyl acetate and dried in vacuum to give **11** as off-white solid (8.4 g, 65%). ^1H NMR (400 MHz, DMSO- d_6): δ 8.93 (d, J = 2.0 Hz, 1H), 8.25 (s, 1H), 7.83 (dd, J = 9.5, 2.0 Hz, 1H), 7.56 (d, J = 9.5 Hz, 1H), 7.47 (d, J = 7.2 Hz, 2H), 7.40 (t, J = 7.2 Hz, 2H), 7.38–7.34 (m, 1H), 5.22 (s, 2H). ESI-MS m/z 331.2 $[\text{M} + \text{H}]^+$.

Step 2: 3-(benzyloxy)-7-((3,5-dimethoxyphenyl)amino)-4H-pyrido[1,2-*a*]pyrimidin-4-one (**12**). A mixture of **11** (1.67 g, 5 mmol), 3,5-dimethoxyaniline (0.92 g, 6 mmol), $\text{Pd}_2(\text{dba})_3$ (0.23 g, 0.25 mmol), (\pm)-BINAP (0.16 g, 0.25 mmol) and cesium carbonate (3.26 g, 10 mmol) in 1,4-dioxane (30 mL) was degassed with N_2 for 10 min. The reaction was heated to 95 °C overnight under N_2 , and then cooled to room temperature. The mixture was filtrated through a Celite, and the filter cake was washed with DCM/MeOH (10/1). After concentration of the filtrate, the residue was purified by column chromatography to give **12** as yellow solid (1.05 g, 52%). ^1H NMR (400 MHz, DMSO- d_6): δ 8.72–8.61 (m, 2H), 8.15 (s, 1H), 7.63 (d, J = 2.2 Hz, 1H), 7.61 (s, 1H), 7.47 (d, J = 7.0 Hz, 2H), 7.39 (t, J = 7.0 Hz, 2H), 7.36–7.30 (m, 1H), 6.33 (d, J = 2.0 Hz, 2H), 6.16 (t, J = 2.0 Hz, 1H), 5.20 (s, 2H), 3.74 (s, 6H). ESI-MS m/z 403.4 $[\text{M} + \text{H}]^+$.

Step 3: 3-(benzyloxy)-7-((3,5-dimethoxyphenyl)(2-(isopropylamino)ethyl)amino)-4H-pyrido[1,2-*a*]pyrimidin-4-one (**13**). To a stirred mixture of 2-methyltetrahydrofuran (12 mL) and KOH (0.336 g, 6 mmol) was added water (0.4 mL). Then **12** (1.6 g, 4 mmol) and tetrabutylammonium bromide (0.322 g, 1 mmol) were added and the mixture was heated at 50 °C for 1 h while stirring. Then *N*-(2-chloroethyl)-2-propanamine hydrochloride (1.14 g, 7.2 mmol) was added in one portion and the mixture was stirred for 18 h at 50 °C. When the conversion was complete, water was added. The mixture was extracted with ethyl acetate twice. The combined organic layer was washed with brine, dried over anhydrous sodium sulfate, and concentrated in vacuum. The residue was purified via silica gel chromatography to afford **13** (1.39 g, 71%). ^1H NMR (400 MHz, DMSO- d_6): δ 8.52–8.47 (m, 1H), 8.15 (s, 1H), 7.56–7.50 (m, 2H), 7.47 (d, J = 7.2 Hz, 2H), 7.40 (t, J = 7.2 Hz, 2H), 7.34 (t, J = 7.2 Hz, 1H), 6.33 (d, J = 2.0 Hz, 2H), 6.28 (t, J = 2.0 Hz, 1H), 5.20 (s, 2H), 3.80 (t, J = 6.7 Hz, 2H), 3.71 (s, 6H), 2.76 (t, J = 6.7 Hz, 2H), 2.74–2.66 (m, 1H), 0.96 (d, J = 6.2 Hz, 6H). ESI-MS m/z 488.6 $[\text{M} + \text{H}]^+$.

Step 4: *tert*-butyl 2-((3,5-dimethoxyphenyl)(3-hydroxy-4-oxo-4H-pyrido[1,2-*a*]pyrimidin-7-yl)amino)ethyl(isopropyl)carbamate (**15**). A mixture of **13** (1.3 g, 2.2 mmol) and trifluoroacetic acid (TFA, 5 mL) was stirred at 90–100 °C for 3 h. Upon completion of the reaction, the mixture was concentrated in vacuum. The residue was dissolved in tetrahydrofuran (13 mL). $(\text{Boc})_2\text{O}$ (0.5 g, 2.3 mmol) and Et_3N (6.4 mL, 46 mmol) were added, and the reaction mixture was stirred at room temperature overnight. TLC detected that the reaction was completed. The mixture was concentrated under vacuum, the residue was purified by column chromatography to afford **15** as light yellow solid (0.56 g, 51%). ^1H NMR (400 MHz, CDCl_3): δ 8.60–8.43 (m, 1H), 8.20 (s, 1H), 7.57–7.40 (m, 2H), 6.45–6.18 (m, 3H), 4.00–3.83 (m, 3H), 3.77 (s, 6H), 3.39 (brs, 2H), 1.44 (s, 9H), 1.15 (d, J = 6.4 Hz, 6H). ESI-MS m/z 498.6 $[\text{M} + \text{H}]^+$.

Step 5: 7-((3,5-dimethoxyphenyl)(2-(isopropylamino)ethyl)amino)-3-(2-methoxyethoxy)-4H-pyrido[1,2-*a*]pyrimidin-4-one (**8a**). A mixture of **22** (50 mg, 0.1 mmol), 1-bromo-2-methoxyethane (12 μL , 0.12 mmol) and K_2CO_3 (42 mg, 0.3 mmol) in DMF (4 mL) was stirred at 90–100 °C for 2 h. Upon completion of the reaction, the reaction mixture was quenched with water and extracted with ethyl acetate twice. The combined extracts were washed with brine, dried over anhydrous Na_2SO_4 and concentrated under vacuum. The resulting residue

was dissolved in DCM (3 mL), TFA (0.5 mL) was added. The resulting solution was stirred at room temperature overnight. After completion (monitored by TLC), the reaction solution was concentrated under reduced pressure. The residue was purified on TLC-preparative plates to afford the desired product **8a** as light yellow oil (31 mg, 80%). ^1H NMR (400 MHz, CDCl_3): δ 8.60 (s, 1H), 8.15 (s, 1H), 7.42 (d, J = 9.7 Hz, 1H), 7.37 (dd, J = 9.7, 2.0 Hz, 1H), 6.27 (s, 3H), 4.39–4.29 (m, 2H), 3.90 (t, J = 6.6 Hz, 2H), 3.82–3.72 (m, 8H), 3.46 (s, 3H), 2.95 (t, J = 6.6 Hz, 2H), 2.89–2.82 (m, 1H), 1.08 (d, J = 6.2 Hz, 6H). HRMS: calculated for $\text{C}_{24}\text{H}_{32}\text{N}_4\text{O}_5$ $[(\text{M} + \text{H})^+]$, 457.2447; found 457.2451.

6.1.4. 7-((3,5-dimethoxyphenyl)(2-(isopropylamino)ethyl)amino)-3-(2-(dimethylamino)ethoxy)-4H-pyrido[1,2-*a*]pyrimidin-4-one (**8b**)

8b was obtained according to the similar procedure of preparing **8a** using *N,N*-dimethylamino chloroethane hydrochloride instead of 1-bromo-2-methoxyethane. Light yellow solid, yield 79%. ^1H NMR (400 MHz, CDCl_3): δ 8.56 (d, J = 2.4 Hz, 1H), 8.09 (s, 1H), 7.41 (d, J = 9.6 Hz, 1H), 7.36 (dd, J = 9.6, 2.4 Hz, 1H), 6.28 (s, 3H), 4.25 (t, J = 5.6 Hz, 2H), 3.92 (t, J = 6.8 Hz, 2H), 3.76 (s, 6H), 2.96 (t, J = 6.8 Hz, 2H), 2.90–2.85 (m, 1H), 2.82 (t, J = 5.6 Hz, 2H), 2.38 (s, 6H), 1.09 (d, J = 6.3 Hz, 6H). ^{13}C NMR (101 MHz, CDCl_3): δ 161.84, 147.57, 143.25, 138.24, 138.13, 137.72, 130.75, 125.91, 111.25, 102.44, 96.74, 68.16, 58.20, 55.47, 52.48, 49.08, 45.59, 45.55, 43.45, 29.70, 22.43. HRMS: calculated for $\text{C}_{25}\text{H}_{35}\text{N}_5\text{O}_4$ $[(\text{M} + \text{H})^+]$, 470.2763; found 470.2766.

6.1.5. 7-((3,5-dimethoxyphenyl)(2-(isopropylamino)ethyl)amino)-3-(2-morpholinoethoxy)-4H-pyrido[1,2-*a*]pyrimidin-4-one (**8c**)

8c was obtained according to the similar procedure of preparing **8a** using 4-(2-chloroethyl)morpholine hydrochloride instead of 1-bromo-2-methoxyethane. Light yellow solid, yield 70%. ^1H NMR (400 MHz, CDCl_3): δ 8.54 (d, J = 2.0 Hz, 1H), 8.08 (s, 1H), 7.41 (d, J = 9.6 Hz, 1H), 7.36 (dd, J = 9.6, 2.0 Hz, 1H), 6.28 (s, 3H), 4.27 (t, J = 5.5 Hz, 2H), 3.96 (t, J = 6.9 Hz, 2H), 3.77–3.73 (m, 10H), 3.00 (t, J = 6.9 Hz, 2H), 2.97–2.90 (m, 1H), 2.85 (t, J = 5.5 Hz, 2H), 2.65–2.57 (m, 4H), 1.12 (d, J = 6.3 Hz, 6H). ^{13}C NMR (101 MHz, CDCl_3): δ 161.87, 153.47, 147.37, 143.24, 138.18, 138.16, 137.84, 130.69, 125.95, 111.10, 102.51, 96.83, 67.57, 66.80, 57.78, 55.49, 55.47, 53.86, 51.93 (2H), 49.30, 43.13, 22.00. HRMS: calculated for $\text{C}_{27}\text{H}_{37}\text{N}_5\text{O}_5$ $[(\text{M} + \text{H})^+]$, 512.2869; found 512.2867.

6.1.6. 7-((3,5-dimethoxyphenyl)(2-(isopropylamino)ethyl)amino)-3-((tetrahydro-2H-pyran-4-yl)oxy)-4H-pyrido[1,2-*a*]pyrimidin-4-one (**8d**)

8d was obtained according to the similar procedure of preparing **8a** using 4-bromotetrahydro-2H-pyran instead of 1-bromo-2-methoxyethane. Light yellow solid, yield 62%. ^1H NMR (400 MHz, CDCl_3): δ 8.59 (d, J = 2.0 Hz, 1H), 8.13 (s, 1H), 7.45 (d, J = 9.6 Hz, 1H), 7.40 (dd, J = 9.6, 2.0 Hz, 1H), 6.29 (s, 3H), 4.75–4.64 (m, 1H), 4.06–4.00 (m, 2H), 3.88 (t, J = 6.7 Hz, 2H), 3.77 (s, 6H), 3.57–3.49 (m, 2H), 2.94 (t, J = 6.7 Hz, 2H), 2.86–2.78 (m, 1H), 2.06–1.19 (m, 2H), 1.88–1.79 (m, 2H), 1.06 (d, J = 6.2 Hz, 6H). HRMS: calculated for $\text{C}_{26}\text{H}_{34}\text{N}_4\text{O}_5$ $[(\text{M} + \text{H})^+]$, 483.2603; found 483.2605.

6.1.7. *tert*-butyl 4-(7-((3,5-dimethoxyphenyl)(2-(isopropylamino)ethyl)amino)-4-oxo-4H-pyrido[1,2-*a*]pyrimidin-3-yl)-3,6-dihydropyridine-1(2H)-carboxylate (**23a**)

Step 1: (E)-5-(((5-bromopyridin-2-yl)imino)methyl)-2,2-dimethyl-1,3-dioxane-4,6-dione (**18**). A mixture of triethyl orthoformate (8.5 g, 0.08 mol) and 2,2-dimethyl-1,3-dioxane-4,6-dione (11.5 g, 0.08 mol) was heated at 60 °C for 2 h. Then a solution of 5-bromopyridin-2-amine (**17**, 13.8 g, 0.08 mol) in

EtOH (80 mL) was added slowly, and the resulting reaction mixture was stirred at 60 °C for additional 2 h. Upon completion of the reaction, the mixture was cooled to room temperature. The precipitate was filtered, and the filter cake was washed with a small amount of EtOH and dried in a vacuum oven to afford **18** as white solid (16.6 g, 64%). ¹H NMR (400 MHz, CDCl₃): δ 11.39–11.24 (m, 1 H), 9.38–9.28 (m, 1 H), 8.47 (d, *J* = 2.4 Hz, 1H), 7.86 (dd, *J* = 8.5, 2.4 Hz, 1H), 6.95 (d, *J* = 8.5 Hz, 1H), 1.76 (s, 6H). ESI-MS *m/z* 327.1 [M+H]⁺.

Step 2: 7-bromo-4H-pyrido[1,2-*a*]pyrimidin-4-one (**19**). Ph₂O was heated to 220 °C, then **18** (16.6 g, 0.051 mol) was slowly added into the solution. The mixture was stirred at 220 °C for 30 min. TLC detected that the reaction was completed. The mixture was cooled and purified by column chromatography to afford **19** (11.5 g, 100%). ¹H NMR (400 MHz, DMSO-*d*₆): δ 9.03 (d, *J* = 2.2 Hz, 1H), 8.32 (d, *J* = 6.4 Hz, 1H), 8.08 (dd, *J* = 9.4, 2.2 Hz, 1H), 7.65 (d, *J* = 9.4 Hz, 1H), 6.46 (d, *J* = 6.4 Hz, 1H). ESI-MS *m/z* 225.0 [M+H]⁺.

Step 3: 7-bromo-3-iodo-4H-pyrido[1,2-*a*]pyrimidin-4-one (**20**). To a stirred solution of **19** (7.4 g, 0.033 mol) in DMF (50 mL) was added NIS (10.4 g, 0.046 mol), the mixture was stirred at 80 °C for 5 h. Upon completion of the reaction, the reaction mixture was cooled to room temperature, and then added with water (50 mL) under stirring. The precipitate was collected by filtration, washed with water dried to a constant weight to afford **20** (12.1 g, 104%). ¹H NMR (400 MHz, DMSO-*d*₆): δ 9.02 (d, *J* = 2.0 Hz, 1H), 8.75 (s, 1H), 8.13 (dd, *J* = 9.4, 2.0 Hz, 1H), 7.67 (d, *J* = 9.4 Hz, 1H). ESI-MS *m/z* 350.9 [M+H]⁺.

Step 4: *tert*-butyl 4-(7-bromo-4-oxo-4H-pyrido[1,2-*a*]pyrimidin-3-yl)-3,6-dihydropyridine-1(2H)-carboxylate (**21a**). **20** (14.1 g, 40 mmol) and *tert*-butyl 4-(4,4,5,5-tetramethyl-1,3,2-dioxaborolan-2-yl)-3,6-dihydropyridine-1(2H)-carboxylate (12.4 g, 40 mmol), Na₂CO₃ (8.5 g, 6 mmol) were dissolved in dioxane (100 mL) and H₂O (25 mL). The suspension was degassed under nitrogen bubbling for 10 min before Pd(dppf)₂Cl₂ (2.9 g, 0.15 mmol) was added. The reaction mixture was heated to 100 °C for 5 h and then diluted with ethyl acetate. The solution was washed with water and brine successively, dried over anhydrous sodium sulfate, and concentrated in vacuum. The residue was purified via silica gel chromatography to afford **21a** (10.7 g, 66%). ¹H NMR (400 MHz, CDCl₃): δ 9.23 (d, *J* = 2.0 Hz, 1H), 8.31 (s, 1H), 7.72 (dd, *J* = 9.4, 2.0 Hz, 1H), 7.53 (d, *J* = 9.4 Hz, 1H), 6.61 (s, 1H), 4.18–4.11 (m, 2H), 3.66 (t, *J* = 5.5 Hz, 2H), 2.63–2.54 (m, 2H), 1.50 (s, 9H). ESI-MS *m/z* 406.1 [M+H]⁺.

Step 5: *tert*-butyl 4-(7-((3,5-dimethoxyphenyl)amino)-4-oxo-4H-pyrido[1,2-*a*]pyrimidin-3-yl)-3,6-dihydropyridine-1(2H)-carboxylate (**22a**). A mixture of **21a** (10.7 g, 26.3 mmol), 3,5-dimethoxyaniline (4.8 g, 31.6 mmol), Pd₂(dba)₃ (2.4 g, 2.63 mmol), (±)-BINAP (2.5 g, 3.95 mmol) and cesium carbonate (12.9 g, 39.5 mmol) in anhydrous toluene (120 mL) was degassed with N₂ for 10 min. The reaction was heated to 100 °C overnight under N₂, and then cooled to room temperature. The mixture was filtrated through a Celite, and the filter cake was washed with DCM/MeOH (10/1). After concentration of the filtrate, the residue was purified by column chromatography to give **22a** (7.1 g, 56%). ¹H NMR (400 MHz, CDCl₃): δ 8.89 (d, *J* = 2.2 Hz, 1H), 8.25 (s, 1H), 7.65 (dd, *J* = 9.6, 2.2 Hz, 1H), 7.59 (d, *J* = 9.6 Hz, 1H), 6.55 (s, 1H), 6.25 (d, *J* = 2.0 Hz, 2H), 6.17 (t, *J* = 2.0 Hz, 1H), 6.10 (s, 1H), 4.15–4.09 (m, 2H), 3.77 (s, 6H), 3.65 (d, *J* = 5.0 Hz, 2H), 2.67–2.56 (m, 2H), 1.49 (s, 9H). ESI-MS *m/z* 479.2 [M+H]⁺.

Step 6: *tert*-butyl 4-(7-((3,5-dimethoxyphenyl)(2-(isopropylamino)ethyl)amino)-4-oxo-4H-pyrido[1,2-*a*]pyrimidin-3-yl)-3,6-dihydropyridine-1(2H)-carboxylate (**23a**). To a stirred mixture of 2-methyltetrahydrofuran (2 mL) and KOH (14 mg,

0.24 mmol) was added water (0.1 mL). Then intermediate **22a** (77 mg, 0.16 mmol) and tetrabutylammonium bromide (13 mg, 0.04 mmol) were added and the mixture was heated at 50 °C for 1 h while stirring. Then *N*-(2-chloroethyl)-2-propanamine hydrochloride (46 mg, 0.29 mmol) was added in one portion and the mixture was stirred for 18 h at 50 °C. When the conversion was complete, water was added. The mixture was extracted with ethyl acetate twice. The combined organic layer was washed with brine, dried over anhydrous sodium sulfate, and concentrated in vacuum. The residue was purified via silica gel chromatography to afford **23a** as yellow solid (55 mg, 61%). ¹H NMR (400 MHz, CDCl₃): δ 8.72 (s, 1H), 8.24 (s, 1H), 7.53–7.44 (m, 2H), 6.55 (s, 1H), 6.30 (s, 3H), 4.13 (brs, 2H), 3.88 (t, *J* = 6.6 Hz, 2H), 3.77 (s, 6H), 3.67 (d, *J* = 5.8 Hz, 2H), 2.93 (t, *J* = 6.6 Hz, 2H), 2.84–2.76 (m, 1H), 2.62 (brs, 2H), 1.50 (s, 9H), 1.05 (d, *J* = 6.2 Hz, 6H). ¹³C NMR (101 MHz, CDCl₃): δ 161.87, 155.77, 154.82, 149.64, 147.60, 146.41, 138.96, 132.21, 130.66, 125.89, 124.53, 115.89, 111.85, 102.65, 96.82, 79.56, 55.41, 55.39, 53.18, 48.80, 43.81, 29.66, 28.48, 27.38, 26.87, 22.96. HRMS: calculated for C₃₁H₄₁N₅O₅ [(M + H)⁺], 564.3182; found 564.3179.

6.1.8. 7-((3,5-dimethoxyphenyl)(2-(isopropylamino)ethyl)amino)-3-(1,2,3,6-tetrahydropyridin-4-yl)-4H-pyrido[1,2-*a*]pyrimidin-4-one (**23b**)

Compound **23a** (85 mg, 0.15 mmol) was dissolved in a solution of HCl/MeOH (4 mL, 4 M in methanol) and the mixture was continually stirred overnight at room temperature. The mixture was concentrated and the residue was purified by silica gel chromatography (dichloromethane/methanol, v/v, 15:1) to give the title product **23b** as yellow solid (38 mg, 55%). ¹H NMR (400 MHz, CDCl₃): δ 8.72 (d, *J* = 1.6 Hz, 1H), 8.25 (s, 1H), 7.51–7.44 (m, 2H), 6.64–6.59 (m, 1H), 6.29 (s, 3H), 3.87 (t, *J* = 6.7 Hz, 2H), 3.77 (s, 6H), 3.63–3.58 (m, 2H), 3.15 (t, *J* = 5.6 Hz, 2H), 2.93 (t, *J* = 6.7 Hz, 2H), 2.83–2.75 (m, 1H), 2.57 (s, 2H), 1.04 (d, *J* = 6.2 Hz, 6H). ¹³C NMR (101 MHz, CDCl₃): δ 161.87, 155.89, 149.62, 147.73, 146.41, 138.82, 132.23, 130.74, 127.06, 125.91, 116.50, 112.11, 102.52, 96.72, 55.44, 55.42, 53.24, 48.81, 45.42, 43.88, 43.08, 29.68, 27.56, 23.01. HRMS: calculated for C₂₆H₃₃N₅O₃ [(M + H)⁺], 464.2657; found 464.2655.

6.1.9. 7-((3,5-dimethoxyphenyl)(2-(isopropylamino)ethyl)amino)-3-(pyridin-3-yl)-4H-pyrido[1,2-*a*]pyrimidin-4-one (**23c**)

23c was obtained according to the similar procedure of preparing **23a** using pyridin-3-ylboronic acid instead of *tert*-butyl 4-(4,4,5,5-tetramethyl-1,3,2-dioxaborolan-2-yl)-3,6-dihydropyridine-1(2H)-carboxylate. Yellow solid, yield 42%. ¹H NMR (400 MHz, CDCl₃): δ 8.98 (d, *J* = 1.8 Hz, 1H), 8.78 (d, *J* = 2.0 Hz, 1H), 8.58 (dd, *J* = 4.8, 1.8 Hz, 1H), 8.48 (s, 1H), 8.26–8.21 (m, 1H), 7.58 (dd, *J* = 9.6, 2.4 Hz, 1H), 7.54 (d, *J* = 9.6 Hz, 1H), 7.41–7.36 (m, 1H), 6.33 (s, 3H), 3.92 (t, *J* = 6.7 Hz, 2H), 3.78 (s, 6H), 2.96 (t, *J* = 6.7 Hz, 2H), 2.88–2.80 (m, 1H), 1.07 (d, *J* = 6.3 Hz, 6H). HRMS: calculated for C₂₆H₂₉N₅O₃ [(M + H)⁺], 460.2344; found 460.2340.

6.1.10. 7-((3,5-dimethoxyphenyl)(2-(isopropylamino)ethyl)amino)-3-(1-methyl-1H-pyrazol-4-yl)-4H-pyrido[1,2-*a*]pyrimidin-4-one (**23d**)

23d was obtained according to the similar procedure of preparing **23a** using 1-methyl-4-(4,4,5,5-tetramethyl-1,3,2-dioxaborolan-2-yl)-1H-pyrazole instead of *tert*-butyl 4-(4,4,5,5-tetramethyl-1,3,2-dioxaborolan-2-yl)-3,6-dihydropyridine-1(2H)-carboxylate. Yellow solid, yield 80%. ¹H NMR (400 MHz, DMSO-*d*₆): δ 8.72 (s, 1H), 8.66 (d, *J* = 2.2 Hz, 1H), 8.37 (s, 1H), 8.12 (s, 1H), 7.66 (dd, *J* = 9.6, 2.2 Hz, 1H), 7.61 (d, *J* = 9.6 Hz, 1H), 6.38 (d, *J* = 2.0 Hz, 2H), 6.33–6.29 (m, 1H), 3.90 (s, 3H), 3.82 (t, *J* = 6.7 Hz, 2H), 3.72 (s, 6H), 2.78 (t, *J* = 6.7 Hz, 2H), 2.75–2.67 (m, 1H), 0.96 (d, *J* = 6.2 Hz,

6H). ^{13}C NMR (101 MHz, DMSO- d_6): δ 161.86, 154.50, 148.47, 148.10, 145.77, 139.17, 136.91, 132.54, 129.57, 126.58, 115.69, 113.27, 108.43, 101.86, 96.29, 55.75, 52.94, 48.52, 44.03, 39.05, 23.33. HRMS calculated for $\text{C}_{25}\text{H}_{30}\text{N}_6\text{O}_3$ [(M + H) $^+$], 463.2453; found, 463.2454.

6.1.11. 7-((3,5-dimethoxyphenyl)(2-(isopropylamino)ethyl)amino)-3-(1,5-dimethyl-1H-pyrazol-4-yl)-4H-pyrido[1,2-a]pyrimidin-4-one (23e)

23e was obtained according to the similar procedure of preparing **23a** using 1,5-dimethyl-4-(4,4,5,5-tetramethyl-1,3,2-dioxaborolan-2-yl)-1H-pyrazole instead of *tert*-butyl 4-(4,4,5,5-tetramethyl-1,3,2-dioxaborolan-2-yl)-3,6-dihydropyridine-1(2H)-carboxylate. Yellow solid, yield 21%. ^1H NMR (400 MHz, CDCl_3): δ 8.71 (s, 1H), 8.49 (s, 1H), 8.03 (s, 1H), 7.51–7.42 (m, 2H), 6.34–6.26 (m, 3H), 3.96 (t, J = 6.6 Hz, 2H), 3.86 (s, 3H), 3.75 (s, 6H), 3.03–2.90 (m, 3H), 2.08 (s, 3H), 1.15 (d, J = 6.2 Hz, 6H). HRMS: calculated for $\text{C}_{26}\text{H}_{32}\text{N}_6\text{O}_3$ [(M + H) $^+$], 477.2610; found 477.2611.

6.1.12. 7-((3,5-dimethoxyphenyl)(2-(isopropylamino)ethyl)amino)-3-(1,3-dimethyl-1H-pyrazol-4-yl)-4H-pyrido[1,2-a]pyrimidin-4-one (23f)

23f was obtained according to the similar procedure of preparing **23a** using 1,3-dimethyl-4-(4,4,5,5-tetramethyl-1,3,2-dioxaborolan-2-yl)-1H-pyrazole instead of *tert*-butyl 4-(4,4,5,5-tetramethyl-1,3,2-dioxaborolan-2-yl)-3,6-dihydropyridine-1(2H)-carboxylate. Yellow solid, yield 54%. ^1H NMR (400 MHz, CDCl_3): δ 8.71 (s, 1H), 8.47 (s, 1H), 8.05 (s, 1H), 7.48 (s, 2H), 6.32–6.25 (m, 3H), 3.98 (t, J = 6.6 Hz, 2H), 3.89 (s, 3H), 3.76 (s, 6H), 3.04–2.91 (m, 3H), 2.44 (s, 3H), 1.12 (d, J = 6.2 Hz, 6H). ^{13}C NMR (101 MHz, CDCl_3): δ 161.91, 155.96, 149.67, 147.35, 146.19, 145.79, 138.77, 132.50, 131.79, 126.08, 112.55, 111.96, 110.19, 102.57, 96.86, 55.48, 55.44, 52.03, 49.29, 43.19, 38.71, 22.05, 14.16. HRMS: calculated for $\text{C}_{26}\text{H}_{32}\text{N}_6\text{O}_3$ [(M + H) $^+$], 477.2610; found 477.2610.

6.1.13. 7-((3,5-dimethoxyphenyl)(2-(isopropylamino)ethyl)amino)-3-(1H-pyrazol-4-yl)-4H-pyrido[1,2-a]pyrimidin-4-one (23g)

Compound **23i** (56 mg, 0.11 mmol) was dissolved in hydrochloric acid solution (4 M in methanol, 3 mL) and the mixture was continually stirred overnight at room temperature. The mixture was concentrated and the residue was purified by silica gel chromatography (dichloromethane/methanol, v/v, 15:1) to give the title product **23g** as yellow solid (35 mg, 71%). ^1H NMR (400 MHz, CDCl_3): δ 8.73 (s, 1H), 8.58 (s, 1H), 8.47 (s, 1H), 8.06 (s, 1H), 7.49–7.35 (m, 2H), 6.39–6.26 (m, 3H), 3.98 (t, J = 6.7 Hz, 2H), 3.79 (s, 6H), 3.06–2.90 (m, 3H), 1.19 (d, J = 6.2 Hz, 6H). HRMS: calculated for $\text{C}_{24}\text{H}_{28}\text{N}_6\text{O}_3$ [(M + H) $^+$], 449.2297; found 449.2302.

6.1.14. 7-((3,5-dimethoxyphenyl)(2-(isopropylamino)ethyl)amino)-3-(1-ethyl-1H-pyrazol-4-yl)-4H-pyrido[1,2-a]pyrimidin-4-one (23h)

23h was obtained according to the similar procedure of preparing **23a** using 1-ethyl-4-(4,4,5,5-tetramethyl-1,3,2-dioxaborolan-2-yl)-1H-pyrazole instead of *tert*-butyl 4-(4,4,5,5-tetramethyl-1,3,2-dioxaborolan-2-yl)-3,6-dihydropyridine-1(2H)-carboxylate. Yellow solid, yield 53%. ^1H NMR (400 MHz, DMSO- d_6): δ 8.78 (s, 1H), 8.69 (s, 1H), 8.39 (s, 1H), 8.22 (s, 1H), 7.76 (dd, J = 9.6, 2.2 Hz, 1H), 7.70 (d, J = 9.6 Hz, 1H), 6.42–6.33 (m, 3H), 3.98–3.89 (m, 5H), 3.81 (t, J = 6.7 Hz, 2H), 3.74 (s, 6H), 2.74 (t, J = 6.7 Hz, 2H), 2.75–2.67 (m, 1H), 1.32–1.28 (m, 3H), 1.02 (d, J = 6.2 Hz, 6H). HRMS: calculated for $\text{C}_{26}\text{H}_{32}\text{N}_6\text{O}_3$ [(M + H) $^+$], 477.2610; found 477.2611.

6.1.15. 7-((3,5-dimethoxyphenyl)(2-(isopropylamino)ethyl)amino)-3-(1-propyl-1H-pyrazol-4-yl)-4H-pyrido[1,2-a]pyrimidin-4-one (23i)

23i was obtained according to the similar procedure of

preparing **23a** using 1-propyl-4-(4,4,5,5-tetramethyl-1,3,2-dioxaborolan-2-yl)-1H-pyrazole instead of *tert*-butyl 4-(4,4,5,5-tetramethyl-1,3,2-dioxaborolan-2-yl)-3,6-dihydropyridine-1(2H)-carboxylate. Yellow solid, yield 42%. ^1H NMR (400 MHz, CDCl_3): δ 8.73 (d, J = 2.0 Hz, 1H), 8.62 (s, 1H), 8.32 (s, 1H), 8.00 (s, 1H), 7.50 (d, J = 9.6 Hz, 1H), 7.46 (dd, J = 9.6, 2.0 Hz, 1H), 6.33–6.27 (m, 3H), 4.14 (t, J = 7.0 Hz, 2H), 3.95 (t, J = 6.7 Hz, 2H), 3.76 (s, 6H), 2.99 (t, J = 6.7 Hz, 2H), 2.93–2.85 (m, 1H), 1.98–1.90 (m, 2H), 1.10 (d, J = 6.4 Hz, 6H), 0.96 (t, J = 7.4 Hz, 3H). HRMS: calculated for $\text{C}_{27}\text{H}_{34}\text{N}_6\text{O}_3$ [(M + H) $^+$], 491.2766; found 491.2767.

6.1.16. 7-((3,5-dimethoxyphenyl)(2-(isopropylamino)ethyl)amino)-3-(1-(2-fluoroethyl)-1H-pyrazol-4-yl)-4H-pyrido[1,2-a]pyrimidin-4-one (23j)

23j was obtained according to the similar procedure of preparing **23a** using 1-(2-fluoroethyl)-4-(4,4,5,5-tetramethyl-1,3,2-dioxaborolan-2-yl)-1H-pyrazole instead of *tert*-butyl 4-(4,4,5,5-tetramethyl-1,3,2-dioxaborolan-2-yl)-3,6-dihydropyridine-1(2H)-carboxylate. Yellow solid, yield 37%. ^1H NMR (400 MHz, CDCl_3): δ 8.74 (d, J = 2.0 Hz, 1H), 8.62 (s, 1H), 8.41 (s, 1H), 8.07 (s, 1H), 7.53–7.45 (m, 2H), 6.34–6.28 (m, 3H), 4.88 (t, J = 4.8 Hz, 1H), 4.76 (t, J = 4.8 Hz, 1H), 4.52 (t, J = 4.8 Hz, 1H), 4.45 (t, J = 4.8 Hz, 1H), 3.90 (t, J = 6.7 Hz, 2H), 3.77 (s, 6H), 2.95 (t, J = 6.7 Hz, 2H), 2.85–2.78 (m, 1H), 1.06 (d, J = 6.2 Hz, 6H). HRMS: calculated for $\text{C}_{26}\text{H}_{31}\text{FN}_6\text{O}_3$ [(M + H) $^+$], 495.2516; found 495.2516.

6.1.17. 7-((3,5-dimethoxyphenyl)(2-(isopropylamino)ethyl)amino)-3-(1-(2-methoxyethyl)-1H-pyrazol-4-yl)-4H-pyrido[1,2-a]pyrimidin-4-one (23k)

23k was obtained according to the similar procedure of preparing **23a** using 1-(2-methoxyethyl)-4-(4,4,5,5-tetramethyl-1,3,2-dioxaborolan-2-yl)-1H-pyrazole instead of *tert*-butyl 4-(4,4,5,5-tetramethyl-1,3,2-dioxaborolan-2-yl)-3,6-dihydropyridine-1(2H)-carboxylate. Yellow solid, yield 39%. ^1H NMR (400 MHz, CDCl_3): δ 8.75 (d, J = 2.0 Hz, 1H), 8.61 (s, 1H), 8.37 (s, 1H), 8.05 (s, 1H), 7.53–7.43 (m, 2H), 6.35–6.25 (m, 3H), 4.36 (t, J = 5.4 Hz, 2H), 3.93–3.88 (m, 2H), 3.81 (t, J = 5.4 Hz, 2H), 3.77 (s, 6H), 3.36 (s, 3H), 2.96 (t, J = 6.7 Hz, 2H), 2.87–2.79 (m, 1H), 1.06 (d, J = 6.2 Hz, 6H). HRMS: calculated for $\text{C}_{27}\text{H}_{34}\text{N}_6\text{O}_4$ [(M + H) $^+$], 507.2716; found 507.2713.

6.1.18. 7-((3,5-dimethoxyphenyl)(2-(isopropylamino)ethyl)amino)-3-(1-(tetrahydro-2H-pyran-2-yl)-1H-pyrazol-4-yl)-4H-pyrido[1,2-a]pyrimidin-4-one (23l)

23l was obtained according to the similar procedure of preparing **23a** using 1-(tetrahydro-2H-pyran-2-yl)-4-(4,4,5,5-tetramethyl-1,3,2-dioxaborolan-2-yl)-1H-pyrazole instead of *tert*-butyl 4-(4,4,5,5-tetramethyl-1,3,2-dioxaborolan-2-yl)-3,6-dihydropyridine-1(2H)-carboxylate. Yellow solid, yield 55%. ^1H NMR (400 MHz, DMSO- d_6): δ 8.78 (s, 1H), 8.65 (d, J = 2.4 Hz, 1H), 8.54 (s, 1H), 8.20 (s, 1H), 7.68 (dd, J = 9.6, 2.4 Hz, 1H), 7.63 (d, J = 9.6 Hz, 1H), 6.39 (d, J = 2.0 Hz, 2H), 6.35–6.28 (m, 1H), 5.49–5.43 (m, 1H), 3.98–3.91 (m, 1H), 3.83 (t, J = 6.6 Hz, 2H), 3.71 (s, 6H), 3.70–3.62 (m, 1H), 2.79 (t, J = 6.6 Hz, 2H), 2.75–2.66 (m, 1H), 2.15–2.05 (m, 1H), 1.98–1.92 (m, 1H), 1.74–1.67 (m, 1H), 1.60–1.53 (m, 1H), 0.96 (d, J = 6.2 Hz, 6H), 0.88–0.83 (m, 2H). HRMS: calculated for $\text{C}_{29}\text{H}_{36}\text{N}_6\text{O}_4$ [(M + H) $^+$], 533.2872; found 533.2875.

6.1.19. 7-((3,5-dimethoxyphenyl)(2-(isopropylamino)ethyl)amino)-3-(1-(tetrahydro-2H-pyran-4-yl)-1H-pyrazol-4-yl)-4H-pyrido[1,2-a]pyrimidin-4-one (23m)

23m was obtained according to the similar procedure of preparing **23a** using 1-(tetrahydro-2H-pyran-4-yl)-4-(4,4,5,5-tetramethyl-1,3,2-dioxaborolan-2-yl)-1H-pyrazole instead of *tert*-butyl 4-(4,4,5,5-tetramethyl-1,3,2-dioxaborolan-2-yl)-3,6-dihydropyridine-1(2H)-carboxylate. Yellow solid, yield 42%. ^1H

NMR (400 MHz, CDCl₃): δ 8.73 (d, J = 2.0 Hz, 1H), 8.63 (s, 1H), 8.40 (s, 1H), 8.02 (s, 1H), 7.54–7.45 (m, 2H), 6.31 (s, 3H), 4.46–4.36 (m, 1H), 4.17–4.10 (m, 2H), 3.92 (t, J = 6.7 Hz, 2H), 3.77 (s, 6H), 3.60–3.52 (m, 2H), 2.96 (t, J = 6.7 Hz, 2H), 2.88–2.81 (m, 1H), 2.19–2.12 (m, 4H), 1.07 (d, J = 6.2 Hz, 6H). HRMS: calculated for C₂₉H₃₆N₆O₄ [(M + H)⁺], 533.2872; found 533.2874.

6.1.20. 7-((3,5-dimethoxyphenyl)(2-(isopropylamino)ethyl)amino)-3-(1-(2-hydroxyethyl)-1H-pyrazol-4-yl)-4H-pyrido[1,2-a]pyrimidin-4-one (**27a**)

Step 1: benzyl 2-((3,5-dimethoxyphenyl)(4-oxo-3-(1-(tetrahydro-2H-pyran-2-yl)-1H-pyrazol-4-yl)-4H-pyrido[1,2-a]pyrimidin-7-yl)amino)ethyl(isopropyl)carbamate (**24**). To a mixture of **23** (1.76 g, 3.3 mmol) and DIEA (2.7 mL, 16.5 mmol) in DCM (20 mL) was added benzyl chloroformate (1.9 mL, 13.2 mmol) dropwise at 0 °C. The mixture was stirred at room temperature for 2 h. Upon completion of the reaction, the reaction mixture was quenched with water and extracted with DCM twice. The combined extracts were washed with brine, dried over anhydrous Na₂SO₄ and concentrated under vacuum. The residue was purified via silica gel chromatography to give **24** as yellow solid (1.5 g, 68%). ¹H NMR (400 MHz, CDCl₃): δ 8.90–8.72 (m, 1H), 8.61 (s, 1H), 8.58–8.46 (m, 1H), 8.08 (s, 1H), 7.68–7.49 (m, 1H), 7.46–7.27 (m, 5H), 6.43–6.13 (m, 3H), 5.43 (dd, J = 9.6, 2.2 Hz, 1H), 5.31–5.18 (m, 2H), 4.43–4.25 (m, 1H), 4.14–4.04 (m, 1H), 4.04–3.84 (m, 2H), 3.82–3.63 (m, 7H), 3.54–3.36 (m, 2H), 2.26–2.15 (m, 1H), 2.15–1.99 (m, 2H), 1.77–1.55 (m, 3H), 1.13 (d, J = 6.2 Hz, 6H). ESI-MS m/z 666.8 [M+H]⁺.

Step 2: benzyl 2-((3,5-dimethoxyphenyl)(4-oxo-3-(1H-pyrazol-4-yl)-4H-pyrido[1,2-a]pyrimidin-7-yl)amino)ethyl(isopropyl)carbamate (**25**). A mixture of **24** (1.5 g, 2.2 mmol) and HCl/MeOH (4 M, 5.5 mL, 22 mmol) was stirred at room temperature overnight. Upon completion of the reaction, the reaction mixture was quenched with saturated aqueous NaHCO₃, then extracted with DCM twice. The combined extracts were washed with brine, dried over anhydrous Na₂SO₄ and concentrated under vacuum to afford the crude product **25** as yellow solid (1.4 g, 109%), which was used in next step without further purification. ESI-MS m/z 582.7 [M+H]⁺.

Step 3: 7-((3,5-dimethoxyphenyl)(2-(isopropylamino)ethyl)amino)-3-(1-(2-hydroxyethyl)-1H-pyrazol-4-yl)-4H-pyrido[1,2-a]pyrimidin-4-one (**27a**). A mixture of **25** (87 mg, 0.15 mmol), (2-bromoethoxy)(*tert*-butyl)dimethylsilane (36 mg, 0.15 mmol) and Cs₂CO₃ (98 mg, 0.3 mmol) in DMF (5 mL) was stirred at 50 °C overnight. After completion (monitored by TLC), the reaction mixture was quenched with water, then extracted with ethyl acetate twice. The combined extracts were washed with water and brine successively, dried over anhydrous Na₂SO₄ and concentrated under vacuum to give **26a**. The residue was dissolved in AcOH (2 mL), HBr (48%, 0.5 mL) was added. The mixture was stirred at room temperature overnight. After completion (monitored by TLC), the solvent was removed under reduced pressure. The residue was basified with saturated aqueous NaHCO₃, then extracted with DCM twice. The combined extracts were washed with brine, dried over anhydrous Na₂SO₄ and concentrated. The residue was purified on TLC-preparative plates to afford the desired product **27a** as yellow solid (15 mg, 20%). ¹H NMR (400 MHz, CDCl₃): δ 8.71 (s, 1H), 8.56 (s, 1H), 8.35 (s, 1H), 8.02 (s, 1H), 7.54–7.45 (m, 2H), 6.37–6.26 (m, 3H), 4.35–4.28 (m, 2H), 4.10–4.02 (m, 2H), 3.91 (t, J = 6.5 Hz, 2H), 3.77 (s, 6H), 2.96 (t, J = 6.5 Hz, 2H), 2.89–2.81 (m, 1H), 1.08 (d, J = 6.2 Hz, 6H). HRMS: calculated for C₂₆H₃₂N₆O₄ [(M + H)⁺], 493.2559; found 493.2558.

6.1.21. 7-((3,5-dimethoxyphenyl)(2-(isopropylamino)ethyl)amino)-3-(1-(2-hydroxy-2-methylpropyl)-1H-pyrazol-4-yl)-4H-pyrido[1,2-a]pyrimidin-4-one (**27b**)

27b was obtained according to the similar procedure of preparing **27a** using 2,2-dimethyloxirane instead of (2-bromoethoxy)(*tert*-butyl)dimethylsilane. Yellow solid, yield 28%. ¹H NMR (400 MHz, CDCl₃): δ 8.74 (s, 1H), 8.62 (s, 1H), 8.37 (s, 1H), 8.06 (s, 1H), 7.54–7.46 (m, 2H), 6.31 (s, 3H), 4.13 (s, 2H), 3.90 (t, J = 6.6 Hz, 2H), 3.77 (s, 7H), 2.95 (t, J = 6.6 Hz, 2H), 2.86–2.78 (m, 1H), 1.25 (s, 6H), 1.06 (d, J = 6.2 Hz, 6H). HRMS: calculated for C₂₈H₃₆N₆O₄ [(M + H)⁺], 521.2872; found 521.2873.

6.1.22. 7-((3,5-dimethoxyphenyl)(2-(isopropylamino)ethyl)amino)-3-(1-(2-(dimethylamino)ethyl)-1H-pyrazol-4-yl)-4H-pyrido[1,2-a]pyrimidin-4-one (**27c**)

27c was obtained according to the similar procedure of preparing **27a** using *N,N*-dimethylamino chloroethane hydrochloride instead of (2-bromoethoxy)(*tert*-butyl)dimethylsilane. Yellow solid, yield 33%. ¹H NMR (400 MHz, CDCl₃): δ 8.74 (d, J = 2.2 Hz, 1H), 8.61 (s, 1H), 8.37 (s, 1H), 8.01 (s, 1H), 7.51 (d, J = 9.6 Hz, 1H), 7.46 (dd, J = 9.6, 2.2 Hz, 1H), 6.31 (s, 3H), 4.30 (t, J = 6.8 Hz, 2H), 3.90 (t, J = 6.7 Hz, 2H), 3.77 (s, 6H), 2.95 (t, J = 6.7 Hz, 2H), 2.86–2.78 (m, 3H), 2.30 (s, 6H), 1.06 (d, J = 6.2 Hz, 6H). ¹³C NMR (101 MHz, CDCl₃): δ 161.92, 155.16, 148.07, 147.58, 145.55, 139.09, 136.51, 131.47, 129.17, 126.09, 115.39, 111.59, 109.22, 102.83, 97.00, 59.13, 55.49, 55.47, 53.07, 50.42, 48.90, 45.61, 45.58, 43.83, 22.89. HRMS: calculated for C₂₈H₃₇N₇O₃ [(M + H)⁺], 520.3032; found 520.3033.

6.1.23. 7-((3,5-dimethoxyphenyl)(2-(isopropylamino)ethyl)amino)-3-(1-(2-morpholinoethyl)-1H-pyrazol-4-yl)-4H-pyrido[1,2-a]pyrimidin-4-one (**27d**)

27d was obtained according to the similar procedure of preparing **27a** using 4-(2-chloroethyl)morpholine hydrochloride instead of (2-bromoethoxy)(*tert*-butyl)dimethylsilane. Yellow solid, yield 41%. ¹H NMR (400 MHz, CDCl₃): δ 8.74 (d, J = 2.0 Hz, 1H), 8.61 (s, 1H), 8.38 (s, 1H), 8.01 (s, 1H), 7.51 (d, J = 9.6 Hz, 1H), 7.47 (dd, J = 9.6, 2.0 Hz, 1H), 6.31 (s, 3H), 4.31 (t, J = 6.7 Hz, 2H), 3.92 (t, J = 6.6 Hz, 2H), 3.77 (s, 6H), 3.73–3.69 (m, 4H), 2.96 (t, J = 6.7 Hz, 2H), 2.89–2.81 (m, 3H), 2.53–2.48 (m, 4H), 1.07 (d, J = 6.2 Hz, 6H). ¹³C NMR (101 MHz, CDCl₃): δ 161.93, 155.14, 148.05, 147.51, 145.57, 139.11, 136.46, 131.49, 129.26, 126.10, 115.43, 111.61, 109.15, 102.84, 97.00, 66.93, 58.26, 55.49, 55.46, 53.68, 52.92, 49.79, 48.97, 43.72, 22.76. HRMS: calculated for C₃₀H₃₉N₇O₄ [(M + H)⁺], 562.3138; found 562.3138.

6.1.24. 7-((3,5-dimethoxyphenyl)(2-(isopropylamino)ethyl)amino)-3-(1-(piperidin-4-yl)-1H-pyrazol-4-yl)-4H-pyrido[1,2-a]pyrimidin-4-one (**27e**)

27e was obtained according to the similar procedure of preparing **27a** using *tert*-butyl 4-iodopiperidine-1-carboxylate instead of (2-bromoethoxy)(*tert*-butyl)dimethylsilane. Yellow solid, yield 25%. ¹H NMR (400 MHz, CDCl₃): δ 8.75 (d, J = 2.0 Hz, 1H), 8.62 (s, 1H), 8.39 (s, 1H), 8.02 (s, 1H), 7.51 (d, J = 9.6 Hz, 1H), 7.47 (dd, J = 9.6, 2.0 Hz, 1H), 6.38–6.25 (m, 3H), 4.34–4.25 (m, 1H), 3.90 (t, J = 6.6 Hz, 2H), 3.77 (s, 6H), 3.35–3.25 (m, 2H), 2.95 (t, J = 6.6 Hz, 2H), 2.86–2.74 (m, 3H), 2.27–2.18 (m, 2H), 2.01–1.97 (m, 2H), 1.06 (d, J = 6.2 Hz, 6H). HRMS: calculated for C₂₉H₃₇N₇O₃ [(M + H)⁺], 532.3032; found 532.3035.

6.1.25. 3-(1-(azetidin-3-yl)-1H-pyrazol-4-yl)-7-((3,5-dimethoxyphenyl)(2-(isopropylamino)ethyl)amino)-4H-pyrido[1,2-a]pyrimidin-4-one (**27f**)

27f was obtained according to the similar procedure of preparing **27a** using *tert*-butyl 3-iodoazetidine-1-carboxylate instead of (2-bromoethoxy)(*tert*-butyl)dimethylsilane. Yellow solid, yield

30%. ^1H NMR (400 MHz, CDCl_3): δ 8.72 (s, 1H), 8.62 (s, 1H), 8.43 (s, 1H), 8.09 (s, 1H), 7.51–7.44 (m, 2H), 6.35–6.25 (m, 3H), 5.00–4.91 (m, 1H), 4.48–4.32 (m, 2H), 3.95–3.89 (m, 2H), 3.80–3.72 (m, 8H), 3.06–2.91 (m, 3H), 1.11 (d, J = 6.2 Hz, 6H). HRMS: calculated for $\text{C}_{27}\text{H}_{33}\text{N}_7\text{O}_3$ [(M + H) $^+$], 504.2719; found 504.2723.

6.1.26. 7-((3,5-dimethoxyphenyl)(2-(isopropylamino)ethyl)amino)-3-(1-(1-methylpiperidin-4-yl)-1H-pyrazol-4-yl)-4H-pyrido[1,2-a]pyrimidin-4-one (29a)

Step 1: benzyl 2-((3,5-dimethoxyphenyl)(4-oxo-3-(1-(piperidin-4-yl)-1H-pyrazol-4-yl)-4H-pyrido[1,2-a]pyrimidin-7-yl)amino)ethyl(isopropyl)carbamate (**28a**). To a solution of *tert*-butyl 4-(4-(7-((2-((benzyloxy)carbonyl(isopropyl)amino)ethyl)(3,5-dimethoxyphenyl)amino)-4-oxo-4H-pyrido[1,2-a]pyrimidin-3-yl)-1H-pyrazol-1-yl)piperidine-1-carboxylate (**26e**, 291 mg, 0.38 mmol) in DCM (5 mL) was added TFA (1 mL). The mixture was stirred at room temperature for 2 h, and then concentrated under vacuum. The residue was basified with ammonia (7 M in methanol) and purified by column chromatography to give the intermediate **28a** as yellow solid (220 mg, 87%). ESI-MS m/z 665.8 [(M + H) $^+$].

Step 2: 7-((3,5-dimethoxyphenyl)(2-(isopropylamino)ethyl)amino)-3-(1-(1-methylpiperidin-4-yl)-1H-pyrazol-4-yl)-4H-pyrido[1,2-a]pyrimidin-4-one (**29a**). To a solution of **28a** (99 mg, 0.15 mmol) in acetonitrile (5 mL) was added formaldehyde solution (37 wt % in water, 61 mg, 0.75 mmol), acetic acid (20 μL) and sodium triacetoxyborohydride (96 mg, 0.45 mmol). The reaction mixture was stirred for 16 h at room temperature. Following this time the reaction mixture was diluted water and saturated aqueous sodium hydrogen carbonate solution. The reaction mixture was extracted with ethyl acetate. The solvent was removed under reduced pressure. The residue was uptaken in AcOH (3 mL) and HBr (48%, 0.5 mL) was added. The mixture was stirred at room temperature overnight. After completion (monitored by TLC), the solvent was removed under reduced pressure. The residue was basified with ammonia (7 M in methanol) and purified by column chromatography to give the intermediate **29a** as yellow solid (8 mg, 10%). ^1H NMR (400 MHz, CDCl_3): δ 8.76–8.70 (m, 1H), 8.61 (s, 1H), 8.38 (s, 1H), 8.01 (s, 1H), 7.53–7.45 (m, 2H), 6.31 (s, 3H), 4.23–4.17 (m, 1H), 3.94 (t, J = 6.8 Hz, 2H), 3.77 (s, 6H), 3.68–3.59 (m, 2H), 3.08–3.01 (m, 2H), 2.97 (t, J = 6.8 Hz, 2H), 2.90–2.83 (m, 1H), 2.37 (s, 3H), 2.25–2.21 (m, 2H), 2.02–1.95 (m, 2H), 1.09 (d, J = 6.2 Hz, 6H). HRMS: calculated for $\text{C}_{30}\text{H}_{39}\text{N}_7\text{O}_3$ [(M + H) $^+$], 546.3188; found 546.3192.

6.1.27. 7-((3,5-dimethoxyphenyl)(2-(isopropylamino)ethyl)amino)-3-(1-(1-ethylpiperidin-4-yl)-1H-pyrazol-4-yl)-4H-pyrido[1,2-a]pyrimidin-4-one (29b)

29b was obtained according to the similar procedure of preparing **29a** using acetaldehyde instead of formaldehyde. Yellow solid, yield 17%. ^1H NMR (400 MHz, CDCl_3): δ 8.74–8.69 (m, 1H), 8.60 (s, 1H), 8.38 (s, 1H), 8.01 (s, 1H), 7.53–7.46 (m, 2H), 6.37–6.27 (m, 3H), 4.31–4.23 (m, 1H), 4.00 (t, J = 6.8 Hz, 2H), 3.77 (m, 6H), 3.67–3.60 (m, 2H), 3.23–3.16 (m, 2H), 3.01 (t, J = 6.8 Hz, 2H), 2.97–2.91 (m, 1H), 2.63–2.59 (m, 2H), 2.33–2.28 (m, 2H), 2.05–1.95 (m, 2H), 1.21–1.17 (s, 3H), 1.14 (d, J = 6.2 Hz, 6H). HRMS: calculated for $\text{C}_{31}\text{H}_{41}\text{N}_7\text{O}_3$ [(M + H) $^+$], 560.3345; found 560.3345.

6.1.28. 3-(1-(1-acetyl)piperidin-4-yl)-1H-pyrazol-4-yl)-7-((3,5-dimethoxyphenyl)(2-(isopropylamino)ethyl)amino)-4H-pyrido[1,2-a]pyrimidin-4-one (29c)

To a mixture of **28a** (100 mg, 0.15 mmol) and Et_3N (84 μL ,

0.6 mmol) in DCM (5 mL) was added acetyl chloride (32 μL , 0.45 mmol) dropwise at 0 $^\circ\text{C}$. Then the reaction mixture was stirred at room temperature for 1 h. Following this time the reaction mixture was diluted water and then extracted with DCM twice. The combined extracts were washed with 0.5 N HCl (aq), dried over anhydrous Na_2SO_4 , and concentrated under reduced pressure. The residue was uptaken in AcOH (3 mL) and HBr (48% in water, 0.5 mL) was added. The mixture was stirred at room temperature overnight. After completion (monitored by TLC), the solvent was removed under reduced pressure. The residue was basified with ammonia (7 M in methanol) and purified by column chromatography to give the intermediate **29c** as yellow solid (41 mg, 48%). ^1H NMR (400 MHz, CDCl_3): δ 8.72 (d, J = 2.0 Hz, 1H), 8.61 (s, 1H), 8.38 (s, 1H), 8.01 (s, 1H), 7.51 (d, J = 9.6 Hz, 1H), 7.47 (dd, J = 9.6, 2.0 Hz, 1H), 6.31 (s, 3H), 4.77–4.71 (m, 1H), 4.46–4.36 (m, 1H), 4.01–3.89 (m, 3H), 3.77 (s, 6H), 3.31–3.22 (m, 1H), 2.97 (t, J = 6.6 Hz, 2H), 2.89–2.75 (m, 2H), 2.29–2.18 (m, 2H), 2.15 (s, 3H), 2.08–1.98 (m, 2H), 1.08 (d, J = 6.2 Hz, 6H). ^{13}C NMR (101 MHz, CDCl_3): δ 169.01, 161.93, 155.11, 148.06, 147.40, 145.54, 139.18, 136.26, 131.44, 126.61, 126.10, 115.40, 111.40, 108.94, 102.92, 97.07, 59.06, 55.49, 55.45, 52.77, 49.00, 45.31, 43.63, 40.51, 32.79, 31.99, 22.66, 21.44. HRMS: calculated for $\text{C}_{31}\text{H}_{39}\text{N}_7\text{O}_4$ [(M + H) $^+$], 574.3138; found 574.3140.

6.1.29. 7-((3,5-dimethoxyphenyl)(2-(isopropylamino)ethyl)amino)-3-(1-(1-(methylsulfonyl)piperidin-4-yl)-1H-pyrazol-4-yl)-4H-pyrido[1,2-a]pyrimidin-4-one (29d)

29d was obtained according to the similar procedure of preparing **29c** using methanesulfonyl chloride instead of acetyl chloride. Yellow solid, yield 45%. ^1H NMR (400 MHz, CDCl_3): δ 8.72 (s, 1H), 8.61 (s, 1H), 8.39 (s, 1H), 8.02 (s, 1H), 7.54–7.45 (m, 2H), 6.35–6.25 (m, 3H), 4.37–4.28 (m, 1H), 3.94–3.90 (m, 3H), 3.77 (s, 6H), 3.02–2.96 (m, 4H), 2.86 (s, 3H), 2.33–2.29 (m, 2H), 2.28–2.18 (m, 4H), 1.09 (d, J = 6.2 Hz, 6H). ^{13}C NMR (101 MHz, CDCl_3): δ 161.96, 155.14, 148.13, 147.42, 145.61, 139.35, 136.35, 131.50, 126.59, 126.16, 115.61, 111.52, 108.88, 102.92 (2H), 97.09, 58.19, 55.51, 55.47, 52.76, 49.07, 44.88, 43.64, 35.69, 31.83, 22.63. HRMS: calculated for $\text{C}_{30}\text{H}_{39}\text{N}_7\text{O}_5\text{S}$ [(M + H) $^+$], 610.2807; found 610.2811.

6.1.30. 3-(1-(1-acetylazetidin-3-yl)-1H-pyrazol-4-yl)-7-((3,5-dimethoxyphenyl)(2-(isopropylamino)ethyl)amino)-4H-pyrido[1,2-a]pyrimidin-4-one (29e)

29e was obtained according to the similar procedure of preparing **29c** using *tert*-butyl 3-iodoazetidine-1-carboxylate instead of *tert*-butyl 4-iodopiperidine-1-carboxylate. Yellow solid, yield 39%. ^1H NMR (400 MHz, CDCl_3): δ 8.69 (s, 1H), 8.60 (s, 1H), 8.44 (s, 1H), 8.07 (s, 1H), 7.49 (t, J = 9.6 Hz, 2H), 6.35–6.27 (m, 3H), 5.21–5.12 (m, 1H), 4.67–4.55 (m, 2H), 4.54–4.42 (m, 2H), 4.01 (t, J = 6.6 Hz, 2H), 3.77 (s, 6H), 3.06–2.93 (m, 3H), 1.96 (s, 3H), 1.15 (d, J = 6.3 Hz, 6H). ^{13}C NMR (101 MHz, CDCl_3): δ 170.78, 162.00, 155.11, 148.27, 147.08, 145.68, 139.26, 137.64, 131.53, 128.45, 126.21, 116.23, 111.42, 108.45, 103.00, 97.29, 57.47, 55.54, 55.51, 55.27, 49.50, 49.44, 43.19, 29.70, 22.00, 19.05. HRMS: calculated for $\text{C}_{29}\text{H}_{35}\text{N}_7\text{O}_4$ [(M + H) $^+$], 546.2825; found 546.2827.

6.1.31. 7-((3,5-dimethoxyphenyl)(2-(isopropylamino)ethyl)amino)-3-(1-(1-(methylsulfonyl)azetidin-3-yl)-1H-pyrazol-4-yl)-4H-pyrido[1,2-a]pyrimidin-4-one (29f)

29f was obtained according to the similar procedure of preparing **29d** using *tert*-butyl 3-iodoazetidine-1-carboxylate instead of *tert*-butyl 4-iodopiperidine-1-carboxylate. Yellow solid, yield 55%. ^1H NMR (400 MHz, CDCl_3): δ 8.56 (s, 1H), 8.41 (s, 1H), 8.29 (s, 1H), 7.95 (s, 1H), 7.55–7.45 (m, 2H), 6.39–6.32 (m, 3H), 5.09–5.02 (m, 1H), 4.38–4.26 (m, 2H), 4.80–3.71 (m, 8H), 3.45–3.38 (m, 2H), 3.22–3.15 (m, 2H), 2.98–2.91 (m, 4H), 1.18 (d, J = 6.2 Hz, 6H). ^{13}C NMR (101 MHz, CDCl_3): δ 162.16, 154.59, 148.38, 145.29, 140.78, 139.50,

136.07, 131.29, 126.29, 126.14, 117.10, 111.57, 107.70, 103.45, 100.00, 55.78, 55.72, 51.11, 47.96, 47.94, 45.17, 41.63, 41.39, 40.39, 22.72. HRMS: calculated for $C_{28}H_{35}N_7O_5S [(M + H)^+]$, 582.2494; found 546.2494.

6.1.32. 7-((cyclopropylmethyl)(3,5-dimethoxyphenyl)amino)-3-(1-methyl-1H-pyrazol-4-yl)-4H-pyrido[1,2-a]pyrimidin-4-one (30a)

To a solution of **22d** (60 mg, 0.16 mmol) in dry DMF (3 mL) at 0 °C was added NaH (13 mg, 0.32 mmol) slowly. After being stirred at 0 °C for 10 min, (bromomethyl)cyclopropane (32 μ L, 0.32 mmol) was added, and the mixture was stirred at room temperature overnight. TLC detected that the reaction was completed. The mixture was quenched with water, then extracted with ethyl acetate twice. The combined extracts were washed with brine, dried over anhydrous Na_2SO_4 and concentrated in vacuum. The residue was purified by column chromatography to afford **30a** as light yellow solid (39 mg, 57%). 1H NMR (400 MHz, $CDCl_3$): δ 8.55 (d, J = 2.6 Hz, 1H), 8.42 (s, 1H), 8.19 (s, 1H), 7.82 (s, 1H), 7.29 (d, J = 9.6 Hz, 1H), 7.20 (dd, J = 9.6, 2.6 Hz, 1H), 6.18–6.04 (m, 3H), 3.96 (s, 3H), 3.62 (s, 6H), 3.41 (d, J = 6.6 Hz, 2H), 0.69–0.60 (m, 1H), 0.38–0.32 (m, 2H), 0.10–0.00 (m, 2H). HRMS: calculated for $C_{24}H_{25}N_5O_3 [(M + H)^+]$, 432.2031; found 432.2033.

6.1.33. 7-((3,5-dimethoxyphenyl)(prop-2-yn-1-yl)amino)-3-(1-methyl-1H-pyrazol-4-yl)-4H-pyrido[1,2-a]pyrimidin-4-one (30b)

30b was obtained according to the similar procedure of preparing **30a** using 3-bromoprop-1-yne instead of (bromomethyl)cyclopropane. Yellow solid, yield 77%. 1H NMR (400 MHz, $CDCl_3$): δ 8.88 (d, J = 2.6 Hz, 1H), 8.62 (s, 1H), 8.32 (s, 1H), 8.00 (s, 1H), 7.53 (d, J = 9.6 Hz, 1H), 7.43 (dd, J = 9.6, 2.6 Hz, 1H), 6.34 (s, 3H), 4.48 (d, J = 2.2 Hz, 2H), 3.97 (s, 3H), 3.77 (s, 6H), 2.37 (d, J = 2.2 Hz, 1H). ^{13}C NMR (101 MHz, $CDCl_3$): δ 161.83, 155.19, 148.05, 147.31, 145.87, 138.04, 136.44, 131.39, 129.77, 126.12, 115.50, 112.56, 109.44, 102.97, 97.57, 77.71, 74.19, 55.47, 42.79, 39.03. HRMS: calculated for $C_{23}H_{21}N_5O_3 [(M + H)^+]$, 416.1718; found 416.1722.

6.1.34. 7-((3,5-dimethoxyphenyl)(2-hydroxyethyl)amino)-3-(1-methyl-1H-pyrazol-4-yl)-4H-pyrido[1,2-a]pyrimidin-4-one (32)

To a solution of **22d** (4.0 g, 10.6 mmol) in DMF (60 mL) was added sodium hydride (60% dispersion in mineral oil, 933 mg, 23.32 mmol) slowly at 0 °C under argon. After being stirred at this temperature for 30 min, (2-bromoethoxy)(*tert*-butyl)dimethylsilane (4.6 mL, 21.2 mmol) was added, and then the reaction mixture was stirred at room temperature overnight. Following this time the reaction mixture was diluted with water and then extracted with ethyl acetate twice. The combined extracts were washed with water and brine, dried over anhydrous Na_2SO_4 , and concentrated under reduced pressure. The residue was dissolved in tetrahydrofuran (20 mL) and tetrabutylammonium fluoride (1 M in tetrahydrofuran, 21.2 mL, 21.2 mmol) was added. The reaction mixture was stirred at room temperature overnight. Following this time the reaction mixture was concentrated under vacuum and the resulting residue was purified by column chromatography to give the title compound **32** as yellow solid (2.5 g, 56%). 1H NMR (400 MHz, $DMSO-d_6$): δ 8.77–8.71 (m, 2H), 8.38 (s, 1H), 8.12 (s, 1H), 7.68 (dd, J = 9.6, 2.6 Hz, 1H), 7.61 (d, J = 9.6 Hz, 1H), 4.96 (t, J = 5.0 Hz, 1H), 3.93–3.83 (m, 5H), 3.71 (s, 6H), 3.68–3.61 (m, 2H). HRMS: calculated for $C_{22}H_{23}N_5O_4 [(M + H)^+]$, 422.1824; found 422.1821.

6.1.35. 7-((2-(cyclopropylamino)ethyl)(3,5-dimethoxyphenyl)amino)-3-(1-methyl-1H-pyrazol-4-yl)-4H-pyrido[1,2-a]pyrimidin-4-one (34a)

Step 1: 2-((3,5-dimethoxyphenyl)(3-(1-methyl-1H-pyrazol-4-yl)-4-oxo-4H-pyrido[1,2-a]pyrimidin-7-yl)amino)ethyl

methanesulfonate (**33**). To a mixture of **32** (2.5 g, 5.9 mmol) and Et_3N (2.1 mL, 14.75 mmol) in DCM (30 mL) was added methanesulfonyl chloride (0.917 mL, 11.8 mmol) dropwise at 0 °C under argon. The reaction mixture was stirred at room temperature for 2 h. After completion (monitored by TLC), the reaction mixture was quenched with water, then extracted with DCM twice. The combined extracts were washed with water and brine successively, dried over anhydrous Na_2SO_4 and concentrated under vacuum. The residue was purified by column chromatography to give **33** (2.2 g, 75%). ESI-MS m/z 499.5 $[M+H]^+$.

Step 2: 7-((2-(cyclopropylamino)ethyl)(3,5-dimethoxyphenyl)amino)-3-(1-methyl-1H-pyrazol-4-yl)-4H-pyrido[1,2-a]pyrimidin-4-one (**34a**). A mixture of **33** (40 mg, 0.08 mmol) and cyclopropylamine (91 mg, 1.6 mmol) in acetonitrile (6 mL) was heated at 100 °C overnight. After completion (monitored by TLC), the reaction mixture was concentrated under vacuum, and the residue was purified on TLC-preparative plates to afford the desired product **34a** as light yellow solid (9 mg, 18%). 1H NMR (400 MHz, $DMSO-d_6$): δ 8.72 (s, 1H), 8.64 (d, J = 2.0 Hz, 1H), 8.36 (s, 1H), 8.11 (s, 1H), 7.66 (dd, J = 9.6, 2.0 Hz, 1H), 7.59 (d, J = 9.6 Hz, 1H), 6.39–6.32 (m, 3H), 3.94 (s, 3H), 3.81 (t, J = 6.8 Hz, 2H), 3.77 (s, 6H), 2.71 (t, J = 6.8 Hz, 2H), 2.33–2.26 (m, 1H), 0.89–0.81 (m, 2H), 0.13–0.02 (m, 2H). HRMS: calculated for $C_{25}H_{28}N_6O_3 [(M + H)^+]$, 461.2297; found 461.2298.

6.1.36. 7-((3,5-dimethoxyphenyl)(2-(oxetan-3-ylamino)ethyl)amino)-3-(1-methyl-1H-pyrazol-4-yl)-4H-pyrido[1,2-a]pyrimidin-4-one (34b)

34b was obtained according to the similar procedure of preparing **34a** using oxetan-3-amine instead of cyclopropylamine. Yellow solid, yield 33%. 1H NMR (400 MHz, $DMSO-d_6$): δ 8.73 (s, 1H), 8.64 (s, 1H), 8.38 (s, 1H), 8.12 (s, 1H), 7.68–7.63 (m, 1H), 7.61 (d, J = 9.6 Hz, 1H), 6.37 (d, J = 1.6 Hz, 2H), 6.33–6.28 (s, 1H), 4.62 (t, J = 6.5 Hz, 2H), 4.31 (t, J = 6.0 Hz, 2H), 3.97–3.86 (m, 4H), 3.81 (t, J = 6.6 Hz, 2H), 3.72 (s, 6H), 2.73 (t, J = 6.6 Hz, 2H). HRMS: calculated for $C_{25}H_{28}N_6O_4 [(M + H)^+]$, 477.2246; found 477.2243.

6.1.37. 7-((3,5-dimethoxyphenyl)(2-((4-hydroxycyclohexyl)amino)ethyl)amino)-3-(1-methyl-1H-pyrazol-4-yl)-4H-pyrido[1,2-a]pyrimidin-4-one (34c)

34c was obtained according to the similar procedure of preparing **34a** using 4-aminocyclohexan-1-ol instead of cyclopropylamine. Yellow solid, yield 41%. 1H NMR (400 MHz, $DMSO-d_6$): δ 8.73 (s, 1H), 8.65 (d, J = 2.4 Hz, 1H), 8.37 (s, 1H), 8.12 (s, 1H), 7.65 (dd, J = 9.6, 2.4 Hz, 1H), 7.61 (d, J = 9.6 Hz, 1H), 6.37 (d, J = 2.0 Hz, 2H), 6.30 (t, J = 2.0 Hz, 1H), 4.42 (d, J = 4.1 Hz, 1H), 3.89 (s, 3H), 3.81 (t, J = 6.6 Hz, 2H), 3.72 (s, 6H), 2.80 (t, J = 6.6 Hz, 2H), 2.34–2.28 (m, 1H), 1.86–1.66 (m, 5H), 1.14–1.06 (m, 2H), 1.04–0.96 (m, 2H). HRMS: calculated for $C_{28}H_{34}N_6O_4 [(M + H)^+]$, 519.2716; found 519.2723.

6.2. Solubility assay

A sufficient amount of sample was added to the PBS buffer (pH 7.4). After 30 min of sonication, the solution was shaken at 37 °C water bath for 24 h to form a supersaturated solution and then filtered by Whatman Unifilter. Concentration of the filtrate was analyzed by HPLC based on the calibration curve of each sample.

6.3. Kinase inhibition assay

Including FGFR1 (Carna, Cat. No. 08–133, Lot. No. 12CBS-0123K), FGFR2 (Carna, Cat. No. 08–134, Lot. No. 13CBS-0735H), FGFR3 (Carna, Cat. No. 08–135, Lot. No. 12CBS-0744 M), FGFR4 (Carna, Cat.

No. 08–136, Lot. No. 12CBS-0076L) and VEGFR2 (Carna, Cat. No. 08–191, Lot. No. 13CBS-0442H) were tested. The concentration gradients from 1.5×10^{-11} to 1.0×10^{-7} mol/L were used for all the test compounds. The experiments were conducted by Sundia MediTech Company, Ltd. (China).

The activity of **23d**, at a concentration of 1 μ M using an ATP concentration of 10 μ M, was screened against a panel of 360 human protein kinases by Eurofins using the Eurofins Kinase Profiler Selectivity Testing Service.

6.4. Molecular docking

The 3D structure of FGFR1 was downloaded from the PDB (<http://www.rcsb.org/>, PDB ID: 5EW8). The protein was prepared with discovery studio 3.1. Molecule **7** and **23d** were built with ChemBio3D and optimized at molecular mechanical level. Then **7** and **23d** were docked to the binding site of JNJ42756493 by employing a protein-ligand docking program GOLD2.5, respectively. Scoring function GOLDScore was used for exhaustive searching, solid body optimizing, and interaction scoring. The final results for molecular docking were visualized by using PyMol program.

6.5. Cell culture and reagents

All cell lines were purchased from National Collection of Authenticated Cell Cultures. Human Gastric Cancer Cell line SNU-16 was cultured in Rosewell Park Memorial Institute (RPMI) 1640 Media (BasalMedia, L210KJ) supplemented with 10% fetal bovine serum (FBS) (GEMINI, 900-108) and Penicillin-Streptomycin (Corning, 30-002-CI) under humidified conditions with 5% of CO₂, 37 °C.

6.6. Cell proliferation assay

SNU-16 cells were seeded in 96-well plates with different cell density, 0.5×10^4 per well for 96 h, 1×10^4 per well for 72 h, 1.5×10^4 per well for 48 h, 2×10^4 per well for 24 h. Different doses of test compounds were treated as soon as the cell seeded in 96-well plates. After indicated times, cell viability was determined by using MTT (CSNpharm, CSN12440) assay. The data was analyzed by using GraphPad Prism 8 software.

6.7. Cell counting assay

SNU-16 cells were seeded in 6-well plates with 1×10^5 per well. The test compounds were treated as soon as the cell seeded in 6-well plates. After indicated time, the images were captured under an inverted microscope. Then resuspended the cells in the captured well, and took counts of the number of living cells by using trypan blue (Biosharp, BL627A) rejection method.

6.8. Cell cycle and apoptosis analysis

The cell cycle and apoptosis analysis were both conducted on flow cytometry (FCM). Cells were seeded in 6-well plates with 1×10^6 per well. The test compounds were administrated as soon as the cell seeded into plates. For cell cycle analysis, the test compounds were treated with 48 h. After the treatment, cells were harvested and washed twice, then fixed by 70% of ethanol. After fixation, washed twice and stained with Cell Cycle detection Kit (KeyGEN, KGA512) according to the manufacturer's protocol. For apoptosis analysis, the test compounds were treated with 72 h, and harvested after administration. Then washed twice and stained by

7-AAD/Annexin-V-PE staining kit (BD Pharmingen, 559763) according to the manufacturer's protocol. The data were analyzed by NovoExpress 1.4.0.

6.9. Immunoblotting analysis

Cells were treated with test compound at indicated time. Then harvested, followed by lysed in $1 \times$ RIPA buffer (Millipore, 20–188), which contained protease inhibitor cocktail (Bimake, B14001) and phosphatase inhibitor cocktail (Bimake, B15001), for 30 min and equalized before loading. The sample were separated on SDS-PAGE gel and transferred onto nitrocellulose filter membranes (Millipore, HATF00010). Then the membranes were incubated with relevant primary antibody and corresponding secondary antibody. Specific protein bands were detected via chemiluminescence detection. The antibodies used in this article were purchased from Cell Signaling Technology (FGFR2, p-FGFR2, AKT, p-AKT, p-FRS2, ERK1/2, p-ERK1/2, caspase 3, cleaved-caspase3), Wanleibio (FRS2) and Abclonal Technology (CDK2, CDK4, CDK6, Cyclin D, Cyclin E, Cleaved-PARP, PARP, β -actin).

6.10. In vivo PK assay

All animal experiments have been approved by the Institutional Animal Care and Treatment Committee of Sichuan University in China. The pharmacokinetic profiles were determined in SD rats. Compound **23d** (12.5% ethanol, 12.5% Kolliphor EL and 75% saline) was subjected to PK studies in SD rats. The test compound was administered via IV at 3 mg/kg and PO at 30 mg/kg. After administration, blood samples were collected. The blood samples were centrifuged to obtain the plasma fraction. The plasma samples were deproteinized with methanol containing an internal standard. After centrifugation, the supernatant was diluted with methanol and centrifuged again. The compound concentrations of the target compound in the supernatant were measured by LC–MS/MS.

6.11. Xenograft mouse studies

Female NOD/SCID mice (6-week-old, weight 18–20 g) in this study were obtained from Beijing HJF bioscience CO. LTD, Beijing, China and maintained in a specific-pathogen-free (SPF) condition facility. A total of 1.0×10^7 SNU-16 Cells in PBS mixed with BD Matrigel (1:1) were inoculated subcutaneously on the right flank of each mouse. When the mean tumor volume had reached approximately 200 mm³, mice were randomly divided into four groups (five mice each): i. vehicle group; ii. 15 mg/kg **23d** group; iii. 30 mg/kg **23d** group; iv. 30 mg/kg erdafitinib group. The test compound was dissolved in ethanol, then mixed with Kolliphor EL, and filled with saline to calculated volume. The formula was 12.5% ethanol, 12.5% Kolliphor EL and 75% saline. Compounds were administrated once per day by oral gavage for 25 days. The tumor volume was measured 3 times per week by using a caliper and calculated according to the following formula: $V = 0.5 \times \text{length} \times \text{width}^2$. Mice were monitored for 25 days. Data are expressed as mean \pm SEM. At the end of study, mice were euthanized, then tumors, blood and organs were extracted. The complete blood count (CBC) and blood biochemical analysis was completed by WestChina-Frontier PharmaTech (WCFP), Chengdu, China. The TGI values were calculated with the following formula: $\text{TGI} = [1 - (T_N - T_0) / (C_N - C_0)] \times 100\%$, T_N and T_0 represent average tumor volume before treatment and that of n days after treatment in indicated group. C_N and C_0 represent average tumor volume before treatment and that of n days after treatment in indicated group, in this study, n is 25th day.

Declaration of competing interest

The authors declare that they have no known competing financial interests or personal relationships that could have appeared to influence the work reported in this paper.

Acknowledgments

We are grateful for Shuhui Xu of State Key Laboratory of Biotherapy (Sichuan University) for NMR measurements and Professor Lijuan Chen's team of State Key Laboratory of Biotherapy (Sichuan University) for HRMS measurements. This work was supported by National S&T Major Special Project on Major New Drug Innovations (2018ZX09201018), National Natural Science Foundation of China (81903441), Sichuan University Postdoctoral Science Research Foundation (2020SCU12020), and Post-Doctor Research Project, West China Hospital, Sichuan University, China (2018HXBH009).

Appendix A. Supplementary data

Supplementary data to this article can be found online at <https://doi.org/10.1016/j.ejmech.2021.113499>.

References

- [1] M. Touat, E. Ileana, S. Postel-Vinay, F. Andre, J.C. Soria, Targeting FGFR signaling in cancer, *Clin. Canc. Res.* 21 (2015) 2684–2694.
- [2] N. Turner, R. Grose, Fibroblast growth factor signalling: from development to cancer, *Nat. Rev. Canc.* 10 (2010) 116–129.
- [3] V.P. Eswarakumar, I. Lax, J. Schlessinger, Cellular signaling by fibroblast growth factor receptors, *Cytokine Growth Factor Rev.* 16 (2005) 139–149.
- [4] A.N. Brooks, E. Kilgour, P.D. Smith, Molecular pathways: fibroblast growth factor signaling: a new therapeutic opportunity in cancer, *Clin. Canc. Res.* 18 (2012) 1855–1862.
- [5] A.A. Belov, M. Mohammadi, Molecular mechanisms of fibroblast growth factor signaling in physiology and pathology, *Cold Spring Harb. Perspect. Biol.* 5 (2013) 239–249.
- [6] D.M. Ornitz, N. Itoh, The fibroblast growth factor signaling pathway, *Wiley Interdiscip. Rev. Dev. Biol.* 4 (2015) 215–266.
- [7] M.V. Dieci, M. Arnedos, F. Andre, J.C. Soria, Fibroblast growth factor receptor inhibitors as a cancer treatment: from a biologic rationale to medical perspectives, *Canc. Discov.* 3 (2013) 264–279.
- [8] N. Hallinan, S. Finn, S. Cuffe, R. Rafee, K. O'Byrne, K. Gately, Targeting the fibroblast growth factor receptor family in cancer, *Canc. Treat. Rev.* 46 (2016) 51–62.
- [9] A.G. Roberto Ronca, Marco Rusnati, Marco Presta, The potential of fibroblast growth factor/fibroblast growth factor receptor signaling as a therapeutic target in tumor angiogenesis, *Expert Opin. Ther. Targets* 19 (2015) 1–17.
- [10] L. Formisano, Y. Lu, A. Servetto, A.B. Hanker, V.M. Jansen, J.A. Bauer, D.R. Sudhan, A.L. Guerrero-Zotano, S. Croessmann, Y. Guo, P.G. Ericsson, K.M. Lee, M.J. Nixon, L.J. Schwarz, M.E. Sanders, T.C. Dugger, M.R. Cruz, A. Behdad, M. Cristofanilli, A. Bardia, J. O'Shaughnessy, R.J. Nagy, R.B. Lanman, N. Solovieff, W. He, M. Miller, F. Su, Y. Shyr, I.A. Mayer, J.M. Balko, C.L. Arteaga, Aberrant FGFR signaling mediates resistance to CDK4/6 inhibitors in ER+ breast cancer, *Nat. Commun.* 10 (2019) 1373.
- [11] R. Dienstmann, J. Rodon, A. Prat, J. Perez-Garcia, B. Adamo, E. Felip, J. Cortes, A.J. Iafrate, P. Nuciforo, J. Tabernero, Genomic aberrations in the FGFR pathway: opportunities for targeted therapies in solid tumors, *Ann. Oncol.* 25 (2014) 552–563.
- [12] T. Helsten, S. Elkin, E. Arthur, B.N. Tomson, J. Carter, R. Kurzrock, The FGFR landscape in cancer: analysis of 4,853 tumors by next-generation sequencing, *Clin. Canc. Res.* 22 (2016) 259–267.
- [13] A. Zehir, R. Benayed, R.H. Shah, A. Syed, S. Middha, H.R. Kim, P. Srinivasan, J. Gao, D. Chakravarty, S.M. Devlin, M.D. Hellmann, D.A. Barron, A.M. Schram, M. Hameed, S. Dogan, D.S. Ross, J.F. Hechtman, D.F. DeLair, J. Yao, D.L. Mandelker, D.T. Cheng, R. Chandramohan, A.S. Mohanty, R.N. Ptashkin, G. Jayakumar, M. Prasad, M.H. Syed, A.B. Rema, Z.Y. Liu, K. Nafa, L. Borsu, J. Sadowska, J. Casanova, R. Bacares, I.J. Kiecka, A. Razumova, J.B. Son, L. Stewart, T. Baldi, K.A. Mullaney, H. Al-Ahmadie, E. Vakiani, A.A. Abeshouse, A.V. Penson, P. Jonsson, N. Camacho, M.T. Chang, H.H. Won, B.E. Gross, R. Kundra, Z.J. Heins, H.W. Chen, S. Phillips, H. Zhang, J. Wang, A. Ochoa, J. Willis, M. Eubank, S.B. Thomas, S.M. Gardos, D.N. Reales, J. Galle, R. Durany, R. Cambria, W. Abida, A. Cercek, D.R. Feldman, M.M. Gounder, A.A. Hakimi, J.J. Harding, G. Iyer, Y.Y. Janjigian, E.J. Jordan, C.M. Kelly, M.A. Lowery, L.G.T. Morris, A.M. Omuro, N. Raj, P. Razavi, A.N. Shoushtari, N. Shukla, T.E. Soumerai, A.M. Varghese, R. Yeager, J. Coleman, B. Bochner, G.J. Riely, L.B. Saltz, H.I. Scher, P.J. Sabbatini, M.E. Robson, D.S. Klimstra, B.S. Taylor, J. Baselga, N. Schultz, D.M. Hyman, M.E. Arcila, D.B. Solit, M. Ladanyi, M.F. Berger, Mutational landscape of metastatic cancer revealed from prospective clinical sequencing of 10,000 patients, *Nat. Med.* 23 (2017) 703–713.
- [14] F. Andre, T. Bachelot, M. Campone, F. Dalenc, J.M. Perez-Garcia, S.A. Hurvitz, N. Turner, H. Rugo, J.W. Smith, S. Deudon, M. Shi, Y. Zhang, A. Kay, D.G. Porta, A. Yovine, J. Baselga, Targeting FGFR with dovitinib (TKI258): preclinical and clinical data in breast cancer, *Clin. Canc. Res.* 19 (2013) 3693–3702.
- [15] S.A. Byron, H. Chen, A. Wortmann, D. Loch, M.G. Gartside, F. Dehkhoda, S.P. Blais, T.A. Neubert, M. Mohammadi, P.M. Pollock, The N550K/H mutations in FGFR2 confer differential resistance to PD173074, dovitinib, and ponatinib ATP-competitive inhibitors, *Neoplasia* 15 (2013) 975–988.
- [16] E. Bello, G. Colella, V. Scarlato, P. Oliva, A. Berndt, G. Valbusa, S.C. Serra, M. D'Incalci, E. Cavalletti, R. Giavazzi, G. Damia, G. Camboni, E-3810 is a potent dual inhibitor of VEGFR and FGFR that exerts antitumor activity in multiple preclinical models, *Canc. Res.* 71 (2011) 1396–1405.
- [17] O.V. Ancker, M. Wehland, J. Bauer, M. Infanger, D. Grimm, The adverse effect of hypertension in the treatment of thyroid cancer with multi-kinase inhibitors, *Int. J. Mol. Sci.* 18 (2017) 625.
- [18] V. Guagnano, A. Kauffmann, S. Wöhrle, C. Stamm, M. Ito, L. Barys, A. Pornon, Y. Yao, F. Li, Y. Zhang, Z. Chen, C.J. Wilson, V. Bordas, M. Le Douget, L.A. Gaither, J. Borawski, J.E. Monahan, K. Venkatesan, T. Brummendorf, D.M. Thomas, C. Garcia-Echeverria, F. Hofmann, W.R. Sellers, D. Graus-Porta, FGFR genetic alterations predict for sensitivity to NVP-BGJ398, a selective pan-FGFR inhibitor, *Canc. Discov.* 2 (2012) 1118–1133.
- [19] P.R. Gavine, L. Mooney, E. Kilgour, A.P. Thomas, K. Al-Kadhimi, S. Beck, C. Rooney, T. Coleman, D. Baker, M.J. Mellor, A.N. Brooks, T. Klinowska, AZD4547: an orally bioavailable, potent, and selective inhibitor of the fibroblast growth factor receptor tyrosine kinase family, *Canc. Res.* 72 (2012) 2045–2056.
- [20] G. Zhao, W.-y. Li, D. Chen, J.R. Henry, H.-Y. Li, Z. Chen, M. Zia-Ebrahimi, L. Bloem, Y. Zhai, K. Huss, S.-b. Peng, D.J. McCann, A novel, selective inhibitor of fibroblast growth factor receptors that shows a potent broad spectrum of antitumor activity in several tumor xenograft models, *Mol. Canc. Therapeut.* 10 (2011) 2200–2210.
- [21] H. Ebiike, N. Taka, M. Matsushita, M. Ohmori, K. Takami, I. Hyohdoh, M. Kohchi, T. Hayase, H. Nishii, K. Morikami, Y. Nakanishi, N. Akiyama, H. Shindoh, N. Ishii, T. Isobe, H. Matsuoka, Discovery of [5-Amino-1-(2-methyl-3H-benzimidazol-5-yl)pyrazol-4-yl]-(1H-indol-2-yl)methanone (CH5183284/debio 1347), an orally available and selective fibroblast growth factor receptor (FGFR) inhibitor, *J. Med. Chem.* 59 (2016) 10586–10600.
- [22] P.C.C. Liu, H. Koblish, L. Wu, K. Bowman, S. Diamond, D. DiMatteo, Y. Zhang, M. Hansbury, M. Rupar, X. Wen, P. Collier, P. Feldman, R. Klabe, K.A. Burke, M. Soloviev, C. Gardiner, X. He, A. Volgina, M. Covington, B. Ruggeri, R. Wynn, T.C. Burn, P. Scherle, S. Yeleswararam, W. Yao, R. Huber, G. Hollis, INCB054828 (pemigatinib), a potent and selective inhibitor of fibroblast growth factor receptors 1, 2, and 3, displays activity against genetically defined tumor models, *PLoS One* 15 (2020).
- [23] T.P.S. Perera, E. Jovcheva, L. Mevellec, J. Vialard, D. De Lange, T. Verhulst, C. Paulussen, K. Van De Ven, P. King, E. Freyne, D.C. Rees, M. Squires, G. Saxty, M. Page, C.W. Murray, R. Gilissen, G. Ward, N.T. Thompson, D.R. Newell, N. Cheng, L. Xie, J. Yang, S.J. Platero, J.D. Karkera, C. Moy, P. Angibaud, S. Laquerre, M.V. Lorenzi, Discovery and pharmacological characterization of JNJ-42756493 (erdafitinib), a functionally selective small-molecule FGFR family inhibitor, *Mol. Canc. Therapeut.* 16 (2017) 1010–1020.
- [24] Y. Lorient, A. Necchi, S.H. Park, J. Garcia-Donas, R. Huddart, E. Burgess, M. Fleming, A. Rezazadeh, B. Mellado, S. Varlamov, M. Joshi, I. Duran, S.T. Tagawa, Y. Zakharia, B. Zhong, K. Stuyckens, A. Santiago-Walker, P. De Porre, A. O'Hagan, A. Avadhani, A.O. Siefker-Radtke, B.L.C.S. Group, Erdafitinib in locally advanced or metastatic urothelial carcinoma, *N. Engl. J. Med.* 381 (2019) 338–348.
- [25] S.M. Hoy, Pemigatinib: first approval, *Drugs* 80 (2020) 923–929.
- [26] S.R. Chandana, H.M. Babiker, D. Mahadevan, Clinical complexity of utilizing FGFR inhibitors in cancer therapeutics, *Expert Opin. Invest. Drugs* 29 (2020) 1413–1429.
- [27] E. Van Cutsem, Y.J. Bang, W. Mansoor, R.D. Petty, Y. Chao, D. Cunningham, D.R. Ferry, N.R. Smith, P. Frewer, J. Ratnayake, P.K. Stockman, E. Kilgour, D. Landers, A randomized, open-label study of the efficacy and safety of AZD4547 monotherapy versus paclitaxel for the treatment of advanced gastric adenocarcinoma with FGFR2 polysomy or gene amplification, *Ann. Oncol.* 28 (2017) 1316–1324.
- [28] P.K. Paik, R. Shen, M.F. Berger, D. Ferry, J.C. Soria, A. Mathewson, C. Rooney, N.R. Smith, M. Cullberg, E. Kilgour, D. Landers, P. Frewer, N. Brooks, F. Andre, A phase Ib open-label multicenter study of AZD4547 in patients with advanced squamous cell lung cancers, *Clin. Canc. Res.* 23 (2017) 5366–5373.
- [29] R. Bahlde, A. Italiano, C. Hierro, A. Mita, A. Cervantes, N. Chan, M. Awad, E. Calvo, V. Moreno, R. Govindan, A. Spira, M. Gonzalez, B. Zhong, A. Santiago-Walker, I. Poggesi, T. Parekh, H. Xie, J. Infante, J. Tabernero, Multicenter phase I study of erdafitinib (JNJ-42756493), oral pan-fibroblast growth factor receptor inhibitor, in patients with advanced or refractory solid tumors, *Clin. Canc. Res.* 25 (2019) 4888–4897.
- [30] K.R. Young Kwang Chae, Peter S. Hammerman, Christos Vaklavas, Nisha Mohindra, Aparna Kalyan, Maria Matsangou, Ricardo, B.C. Costa, Victoria M. Villafior, Massimo Cristofanilli, Francis J. Giles, Inhibition of the fibroblast growth factor receptor (FGFR) pathway: the current landscape and barriers to clinical application, *Oncotarget* 8 (2017) 16052–16074.

- [31] T.D.B. Harshnira Patani, Nethaji Thiyagarajan, Richard A. Norman, Ogg Derek, Jason Breed, Ashford Paul, Andrew Potterton, Mina Edwards, Sarah V. Williams, Gary S. Thomson, S. Camilla, M. Pang, Margaret A. Knowles, Alexander L. Breeze, Christine Orengo, Chris Phillips, Matilda Katan, Landscape of activating cancer mutations in FGFR kinases and their differential responses to inhibitors in clinical use, *Oncotarget* 7 (2016) 24252–24268.
- [32] I.S. Babina, N.C. Turner, Advances and challenges in targeting FGFR signalling in cancer, *Nat. Rev. Canc.* 17 (2017) 318–332.
- [33] M. Katoh, Fibroblast growth factor receptors as treatment targets in clinical oncology, *Nat. Rev. Clin. Oncol.* 16 (2019) 105–122.
- [34] W. Cheng, M. Wang, X. Tian, X. Zhang, An overview of the binding models of FGFR tyrosine kinases in complex with small molecule inhibitors, *Eur. J. Med. Chem.* 126 (2017) 476–490.
- [35] F.T. Liu, N.G. Li, Y.M. Zhang, W.C. Xie, S.P. Yang, T. Lu, Z.H. Shi, Recent advance in the development of novel, selective and potent FGFR inhibitors, *Eur. J. Med. Chem.* 186 (2020) 111884.
- [36] A. Markham, Erdafitinib: first global approval, *Drugs* 79 (2019) 1017–1021.
- [37] a) . <https://cstnprodstorage.blob.core.windows.net/pdfs/ErdafitinibPK.pdf>;
b) . <https://www.rxlist.com/balversa-drug.htm>.
- [38] P. R. Angibaud, O. A. Querolle, I. N. C. Pilatte, L. Meerpoel, V. S. Poncelet, Quinazolinone derivatives useful as FGFR kinase modulators, *PCT Int. Appl* (April 26, 2013). WO 2014/174307 A1.
- [39] J.R. Somoza, D. Koditek, A.G. Villaseñor, N. Novikov, M.H. Wong, A. Licican, W. Xing, L. Lagpacan, R. Wang, B.E. Schultz, G.A. Papalia, D. Samuel, L. Lad, M.E. McGrath, Structural, biochemical, and biophysical characterization of idelalisib binding to phosphoinositide 3-kinase delta, *J. Biol. Chem.* 290 (2015) 8439–8446.
- [40] G.W. Collie, C.M. Koh, D.J. O'Neill, C.J. Stubbs, P. Khurana, A. Eddershaw, A. Snijder, F. Mauritzson, L. Barlind, I.L. Dale, J. Shaw, C. Phillips, E.J. Hennessy, T. Cheung, A.J. Narvaez, Structural and molecular insight into resistance mechanisms of first generation cMET inhibitors, *ACS Med. Chem. Lett.* 10 (2019) 1322–1327.
- [41] R. Jorda, S. Krajčovičová, P. Králová, M. Soural, V. Kryštof, Scaffold hopping of the SYK inhibitor entospletinib leads to broader targeting of the BCR signalosome, *Eur. J. Med. Chem.* 204 (2020) 112636.
- [42] G. Saxty, C. W. Murray, V. Berdini, G. E. Besong, C. C. Hamlett, C. N. Johnson, S. J. Woodhead, M. Reader, D. C. Rees, L. A. Mevellec, P. R. Angibaud, E. J. Freyne, T. C. Govaerts, J. E. Weerts, T. P. Perera, R. A. Gilissen, B. Wroblowski, J. F. Lacrampe, A. Papanikos, O. A. Querolle, E. T. Pasquier, I. N. Pilatte, P. G. Bonnet, W. C. Embrechts, R. Akkari, L. Meerpoel, Pyrazolyl quinazoline kinase inhibitors, *PCT Int. Appl* (April 30, 2010). WO 2011/135376 A1.